

A Balancing and Monitoring System for Battery Cell Stacks in Electrical Vehicles

Olov Ershag

Luleå University of Technology

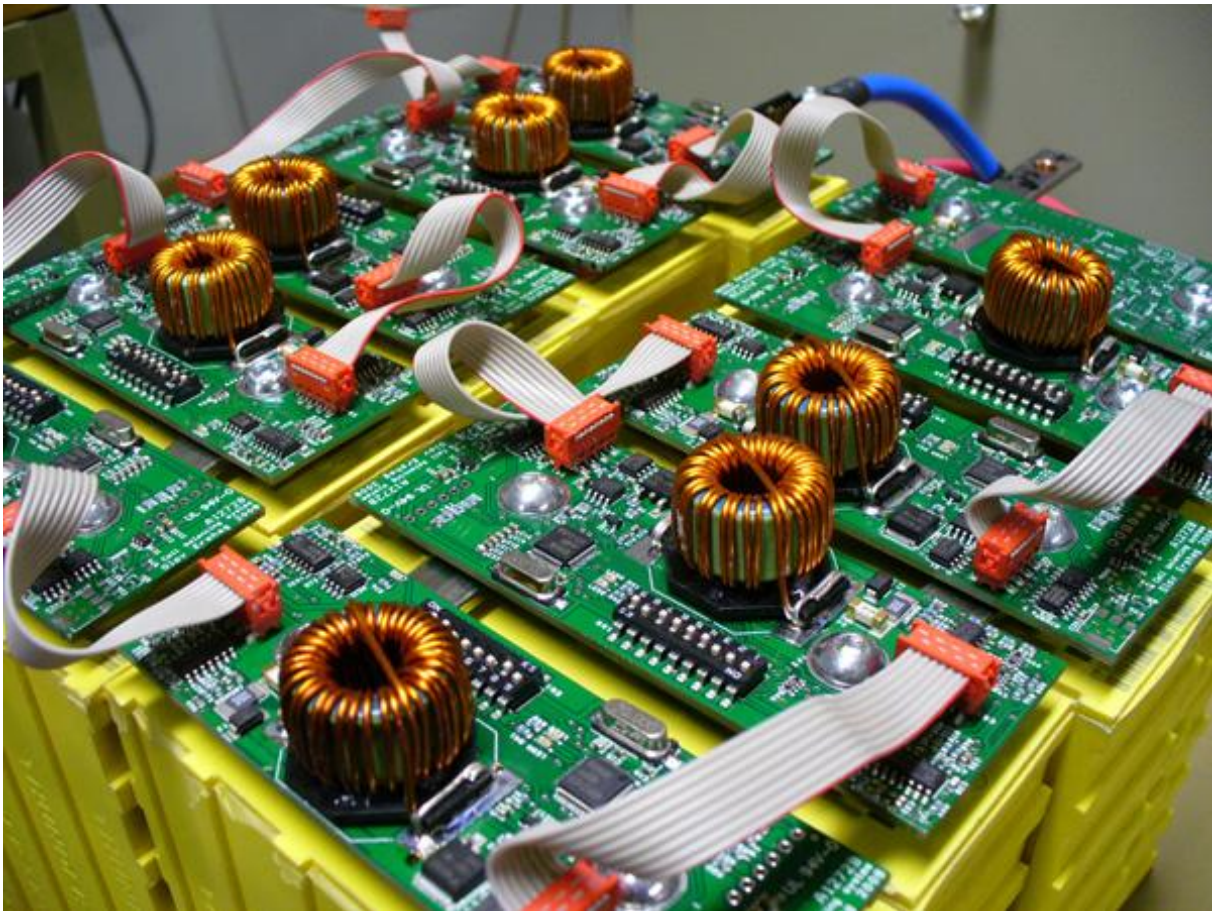
MSc Programmes in Engineering
Electrical Engineering

Department of Computer Science and Electrical Engineering
Division of EISLAB

A balancing and monitoring system for battery cell stacks in electrical vehicles

Olov Ershag

X7002E – Master Thesis in Electrical Engineering



Preface

The Van de Wiele group consists of leading companies in, among other things, technology for weaving machines. Aros Electronics AB (hereby Aros) is a company located in Mölndal, Sweden which is part of this group as a production center and has specialized in motor controllers, sensors and field buses (1). Aros also has its own development unit working with designing new circuit boards and software. There are about hundred employees in Mölndal and the company often has youths for summer jobs and master theses.

As a spare time project, Aros has bought a moped that will be modified by counterchanging the combustion engine with a brushless electrical motor with one of their motor controllers. The moped will also be equipped with a battery pack consisting of ten lithium ion battery cells at 40 Ah each. The battery pack will be able to hold about 1.4 kWh of energy. My task has been to develop and construct a cell balancing and monitoring system for these batteries.

The purpose of this project is to create a demonstration object to show at fairs and other kinds of events, but also to gain knowledge in the field since many employees at Aros are interested in building their own electrical vehicle. The concept of lithium ion battery stacks is not only applicable in the automotive industry; it can also be useful on many other kinds of applications where energy storage is necessary. There is still development going on in the lithium ion battery field, but it has already been accepted as a very beneficial type of battery since it has a good energy to weight and volume ratio. The drawback of lithium ion batteries is that they can be of danger to people and objects due to its chemical contents. It is also sensitive to ambient temperature. This is why an advanced battery control system has to be used together with this type of batteries.

My work at Aros started in June 2008 and ended in November 2008. Although the moped was not ready for ride at the end of my work, all the separate systems seems to work and the only thing remaining is the mechanical assembly.

I have received great support from the employees at Aros. I would foremost like to give my thanks to my mentors, see Appendix 8 , but also to all helpful personnel I have come in contact with. I would like to mention some of them by name:

Andreas Johansson – For assistance with the hardware development and circuit design.

Marie Wide and **Björn Gunnarsson** – For assistance with the OrCad Layout program and how to use Aros' database with electrical components.

Conny Dagerot and **Niklas Wahlgren** – For assistance with the software programming using Aros own object oriented operative system, ArOS.



Olov Ershag, author

Abstract

In this report, different methods for balancing and monitoring battery cells are discussed and evaluated. The chosen method is built in a modular approach which enables the system to be extended to any number of cells. The goal has also been to make the system cheap and simple, but still powerful and efficient.

During the summer and autumn semester 2008 the system was designed, constructed and tested by the author at Aros Electronics AB located in Mölndal, Sweden. The cell balancing and monitoring functionality was needed in an electrical demonstration vehicle together with Aros' electrical motor and motor controller.

The system is able to determine the state of charge of the battery cells by measuring their voltage with an accuracy of about 10 mV. It is also able to transfer charge between two adjacent cells with a power of up to 11.5 W and with an efficiency of up to 80 %.

Nine cards were created for the lithium ion battery stack of ten cells. The cards communicate with each other and a superior control system via the digitally isolated controller area network bus, providing high speed and reliability for use in automotive environments with much electromagnetic interference.

Table of Contents

Introduction	6
Theory	8
Lithium ion batteries vs. other types	8
Techniques for cell balancing	9
Using resistors in parallel	9
Transferring energy	10
Measuring cell voltages	14
Using a transformer	14
Measuring the balancing current.	16
Driving transistors	18
Communication with other modules	18
Evaluation	20
Measuring voltages	20
In theory	20
In practice	21
The influence of current flow	22
Measuring balancing current	24
In theory	24
In practice	24
Driving transistors	25
Dead time	26
Gate resistances.	26
Temperature measurement	27
Protection	29
Over current	29
Over voltage	30
The micro controller, R8C23	31
Complementary pulse width modulation, PWM	32
Analog to digital converter, ADC	33
Pulse Output Forced Cutoff	34
Software	35
Programming	35
Aros operating system, ArOS	35
Floating point arithmetic	35
Digital filters	37
Current regulator	39
CAN communication	40
Efficiency	42
Losses breakdown	42
Resistances	43

<i>Discussion</i>	45
Determining the state of charge	45
Measuring the cell voltages	45
Current measurements	46
Transistor losses	46
Budget	47
CAD	47
<i>References</i>	48
<i>Appendix</i>	49

Introduction

Electrical vehicles and hybrid electrical vehicles, HEV, have begun to take a large space in the automotive type of business. Electrical motors are far more energy efficient than conventional combustion engines running on petrol or diesel. The high price on oil as well as the awareness of environmental consequences of carbon dioxide emissions has forced the automotive manufactures to look at other energy sources. Although the modern car still may have a combustion engine, my guess is that it will not be very powerful. The engine will only be powerful enough to run the car on highways at constant speed. For acceleration, there will be an electrical motor that can deliver the extra power required.

The electrical motor can not only be used to make the car accelerate faster, it can also be used to convert the kinetic energy of a moving car to electrical energy and store it in an energy buffer for later use. This is a major part in reducing the petrol consumption.

Imagine a 1.8 ton car running at 110 km/h and also imagine that the car has to make a sudden brake. The brake discs will heat with 210 000 W during the four seconds it takes to stop the car. If the energy instead could be stored in the car, it could be used to accelerate the car back to 110 km/h, disregarding losses.

To be able to handle this magnitude of energy and power, large batteries have to be used. Not only must the batteries be able to hold all the energy, but they also have to be able to deliver and receive the power when accelerating and breaking. Another problem is that batteries have mass and volume. The weight of the vehicle is of importance in many aspects and there may not be much room to keep large batteries in the vehicle.

Lithium ion batteries have revolutionized the energy storage market and have many benefits that will be discussed later in this report. However, there are some problems with this kind of batteries. The cell voltage in each cell has to be between 2.5 and 4.25 V. If the voltage drops below 2.5 V the cell loses its ability to store energy and if the voltage rises above 4.25 V the electrolyte will start to vaporize and pressure inside the cell will build up. This can cause the battery to swell or even explode and catch fire. It is therefore important to have a battery management system, BMS, to monitor the voltages and report to a supervision system if the cell voltage gets out of range.

Since the cell voltage is low, many cells have to be connected in series to increase the voltage up to 48 V or even up to 300 V to drive electrical motors in HEV. When having battery cells in a stack it is important to keep all cell voltages equal. A difference in inner cell series resistances and temperature changes causes the cells voltages to vary differently in a long period of time. If, for example, the first cell in a stack of two cells is at 2.5 V and the second at 4.25 V, the stack cannot be charged anymore because it will cause the voltage of the second cell to go above 4.25 V. Neither can the stack be discharged because it will cause the voltage of the first cell to go below 2.5 V. Even though there is energy left in the battery stack it is not allowed to extract it.

The solution to this problem is to keep the battery stack balanced. This is the task of the battery management system. There are many different kinds of strategies when designing a BMS and some of them will be subjects for discussion in this report.

The purpose of this work is to gain knowledge in the field of energy storage in vehicles and to find an efficient, simple and cheap way to keep cells in a battery stack balanced and monitored.

The field of balancing battery cells is quite big. Therefore there have to be limits in the thesis. The approach is to find a BMS that is flexible and easily adjusted to different types of batteries or ultra capacitors as well as different number of cells in the stack. Preferable, there should also be a way to estimate the state of charge, SoC, in the stack.

This work will not include the construction of a charger for the battery stack due to the difficulties in constructing a primary switched circuit with current limiting and over temperature protection. That is a master's thesis on its own.

There will not be any kind of series switch for disconnecting the battery stack from the motor in case of over current or similar. This will require an additional circuit board or it may be implemented by connection a relay to the motor controller circuit board. The principle of connection between the battery pack and the electrical motor can be seen in Figure 1.

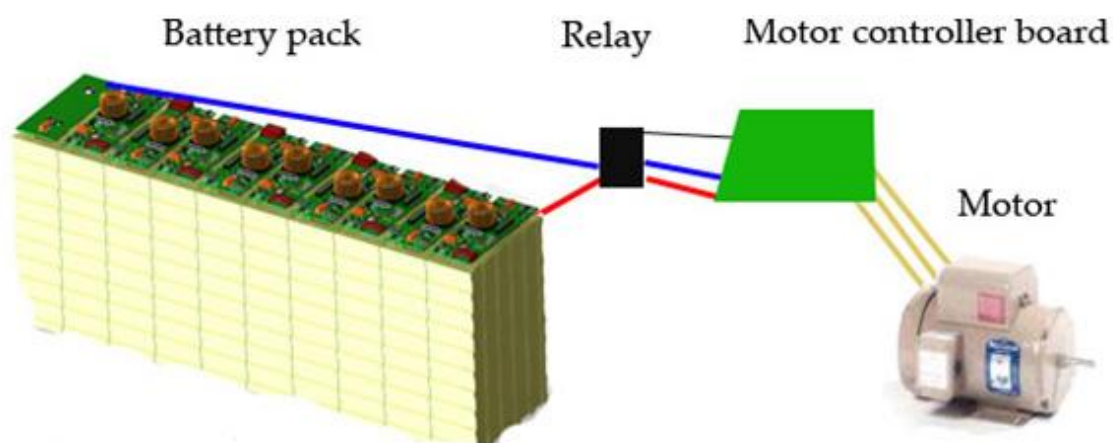


Figure 1. The connection between the battery pack, the motor controller board and the motor. The relay may be omitted.

The work will focus on designing an efficient, simple and not too expensive way to balance and monitor the cells in the battery stack.

Theory

Lithium ion batteries vs. other types

Although Aros already had decided which batteries to use for this project, there are some things to be said about choosing the type of energy storage.

Thunder Sky Battery Limited is a company in China that has developed a quite safe lithium ion battery cell that is recommended for use in automotive vehicles. This battery cell type, LFP, has a positive pole of LiFePO_4 . Even if the cells are over charged or over discharged, they will not cause danger to people; they will not burn or smoke as battery cells with a pole of LiFCoO_2 or LiFNiMnO_2 can (2). This is the reason for choosing the LFP battery cells for this project.

Lithium ion batteries have indeed the best performance in energy/weight and energy/volume ratios, but they are still too expensive and unsafe to be accepted by the industry. Lead acid batteries are still dominating due to their low price (3). A quick comparison between the lithium ion batteries used in this project (LFP 40Ah) and other types of energy buffers can be seen in Table 1.

Table 1. A comparison between different kinds of energy storage units (4).

	Thunder sky LFP 40 Ah	Clas Ohlson lead-acid 7,2 Ah	Maxwell Ultra Cap 94 F, 75 V
Energy/weight [Wh/kg]	132	93	2.2
Energy/volume [Wh/l]	85	37	2.3
Discharge rate per month	3 %	20 %	50 %
Cycles (80% of capacity)	2000	600	1 000 000

The numbers in the above table is taken from batteries that come off the shelf. There are of course new batteries of the same type, but with better performance. There are lithium ion polymer batteries performing up to 400 Wh/Kg and 500 Wh/l.

Techniques for cell balancing

There have been much research in the area of cell balancing and there are many different approaches to choose from. Should it be light-weight, inexpensive, flexible to different kinds of set-ups, efficient or all together?

Using resistors in parallel

The cheapest and most simple way to balance cells is to put resistors of equal resistance in parallel with each cell according to Figure 2. The resistors should be chosen so that the leakage current through them are two to ten times bigger than the leakage current through the battery depending on the desired accuracy. The big draw-back of this solution is that the batteries will constantly discharge over the resistors, but if the current drawn from the batteries is big compared to the current through the resistors it might be an option.

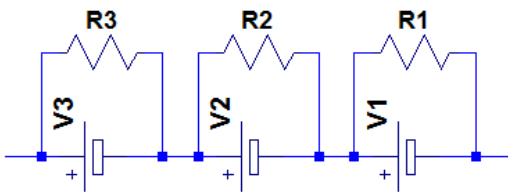


Figure 2. Passive cell balancing using resistors in parallel with each cell.

An extension to this approach is to monitor the cell voltage and activate a transistor to discharge the battery if its voltage is above a certain threshold value. This demands some more circuitry with a voltage comparator and a reference voltage. The resistor should be a high power resistor to be able to dissipate the energy from the battery charger when the battery is full. The circuit set-up for this method is illustrated in Figure 3.

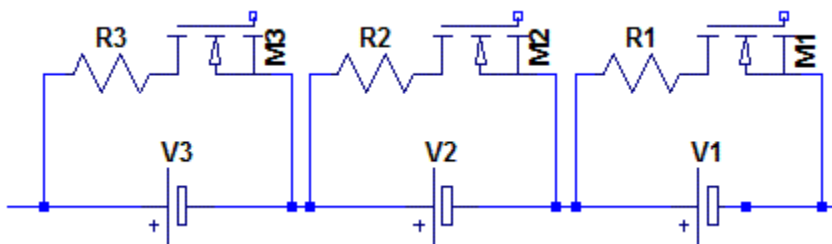


Figure 3. Active cell balancing with discharge transistors.

This method is more efficient since it only discharge the cells if their voltage is too high. The power needed to drive the active circuits and MOSFET drivers should be negligible. There are also disadvantages; if all cells in the stack are fully charged except one, the efficiency in charging the last cell will only be 10% in a stack of ten cells. The heat generated will be substantial if large cells are used and the charging power is 500 W.

Both methods above are using the dissipative method and turns the energy from the cells to heat to keep the battery balanced. This method is cheap and simple, but it could be desirable to have a more efficient approach.

Transferring energy

A much more energy efficient way of balancing cells is to transfer energy from the cells with higher SoC to the less charged cells. To accomplish this task, it is necessary to use some kind of temporary energy buffer to store energy. Usually this is either a capacitor or an inductor. Some of the techniques will be listed here.

Using capacitors

The general principle of using capacitors as energy buffers can be viewed in Figure 4. If V_2 has higher voltage than V_1 , the transistor switches named $M_{x'}$ are first closed, allowing C_1 to charge to the same voltage as V_2 . These transistors are then opened and the M_x transistor switches are closed. This will release the charge stored in C_1 over V_1 and thus charging V_1 .

The downside of using capacitors is that series resistances have to be used to limit the current flowing to and from the capacitor. This reduces the efficiency a lot. Also, it requires a more advanced transistor driver since the transistor source voltages change over time.

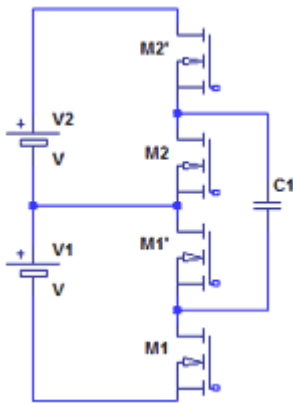


Figure 4. Using the capacitor, C_1 , as energy buffer for transferring energy between V_1 and V_2 .

Buck-Boost conversion

The buck-boost concept implies boosting voltage to a higher value. The circuit in Figure 5 shows the circuit. The cell with the highest voltage is located and energy from that cell is transferred upstream. If B_N has the highest voltage, S_N will be closed to build up a current through L_N . S_N will then open and the current will have to flow through D_N , charging all the above battery cells, B_1 to B_{N-1} . If instead B_1 has the highest voltage, its energy will be diverted in a similar way to the underlying cells, B_2 to B_N , using S_1 , L_1 and D_1

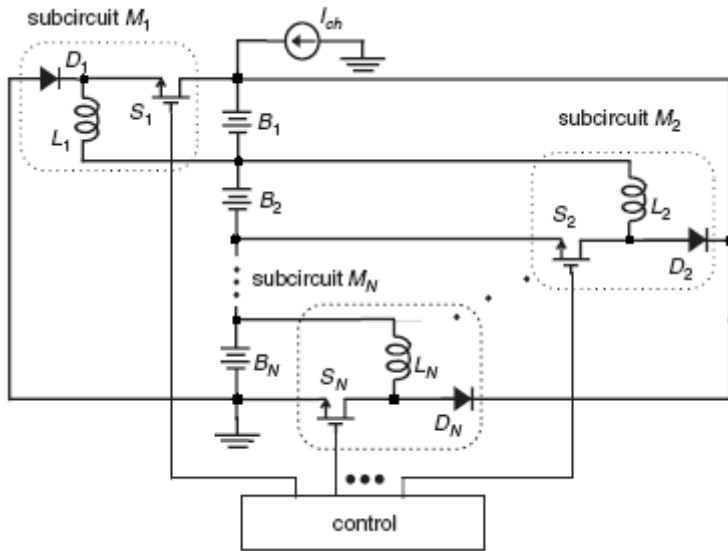


Figure 5. A cell charge equalization circuit utilizing the buck-boost concept.

The advantages with this method are that it is almost non-dissipative and that it quite easily can be modified for different numbers of cells in the battery.

The disadvantages are difficulties in driving the transistors and measuring each cell voltage if the number of cells grows, since this implies a high common mode voltage. The consequence of using this method is that charge could be transferred back and forth to a single cell under special circumstances. Also, if the number of cells would be extended it may be necessary to change the whole control unit.

More information about this method can be found in (5) and a similar method using transformers and capacitors is described in (6).

Using a multi-winded transformer

This method is the opposite of the previous; it takes energy from the whole cell stack and transfers it to the single cell with the least voltage. The principle of operation can be seen in Figure 6. M1 is switched and the cell with the least voltage will clamp the secondary transformer voltage. This implies that the current will flow only to the cell with the least voltage.

With this circuit, one can be sure that the cells will be properly balanced, but one also suffers from the problem of transferring energy back and forth from cells. In the case of expanding the number of cells, a new transformer has to be constructed.

Power will mainly be lost in the diodes, but also in the transformer. Problems can arise since the diodes have different forward voltage drops at different temperatures and the diodes might get heated when they are conducting big currents.

More information around a similar concept can be found in (7).

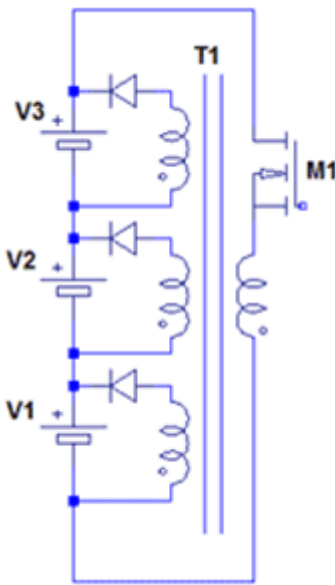


Figure 6. Cell balancing with a circuit using a multi-winded transformer, T1. The circuit is simplified for simplicity.

A modular approach

This is the concept that has been implemented in this project. It is a modular design which can be used with any number of cells. One module consists mainly of two transistors and one inductor which can be seen in Figure 7. It is a further development of the work described in (8).

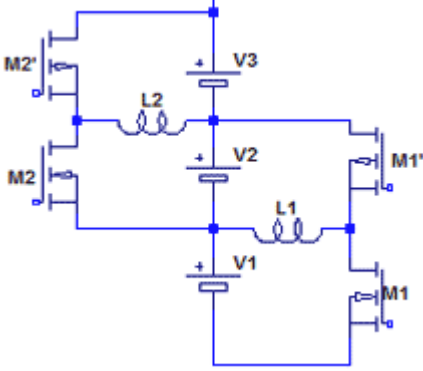


Figure 7. A modular concept of cell balancing using transistors and an inductor to transfer energy between cells. The figure shows two modules that shares the second cell, V2. The number of modules will equal the number of cells in the stack minus one. This is the concept used in this project.

A module compares the voltages in the two cells it is connected to and transfers energy from the cell with higher voltage to the one with lower voltage. The number of modules will be equal to the number of cells minus one. M_N and M_N' are activated with a complementary pulse width modulated, PWM, gate-drive signal. By adjusting the duty cycle of this signal, the current through L_N can be freely controlled to both positive and negative values.

If, for example, V_2 has a higher voltage than V_1 , $M1'$ will first be closed to build up a current through the upper loop ($M1'$, $L1$, and V_2). When the PWM signal then goes low, $M1'$ will be opened and $M1$ will be closed, allowing the built up current to flow in the lower loop ($L1$, $V1$, and $M1$) which will charge $V1$. Thus, energy has been transferred from V_2 to $V1$.

This method will be described in detail throughout this report.

Measuring cell voltages

There is a problem in measuring cell voltages when the number of cells grows. This is due to the high common mode voltage which can be up to several hundreds of volts in modern HEV. A solution to the problem is to use galvanic or optical isolation between the cells and the measuring unit.

Using a transformer

There exists a method similar to the previous described method, *Using a multi-winded transformer*. This method has been further discussed in (9) and I have also made simulations to verify the concept.

The principle of operation is described in Figure 8. This method works fairly well, but it can be difficult to get the required accuracy due to, among other things, the differences in the forward voltage drop over the diode. It also requires a transformer for each cell and some kind of switch system for choosing which cell voltage to measure.

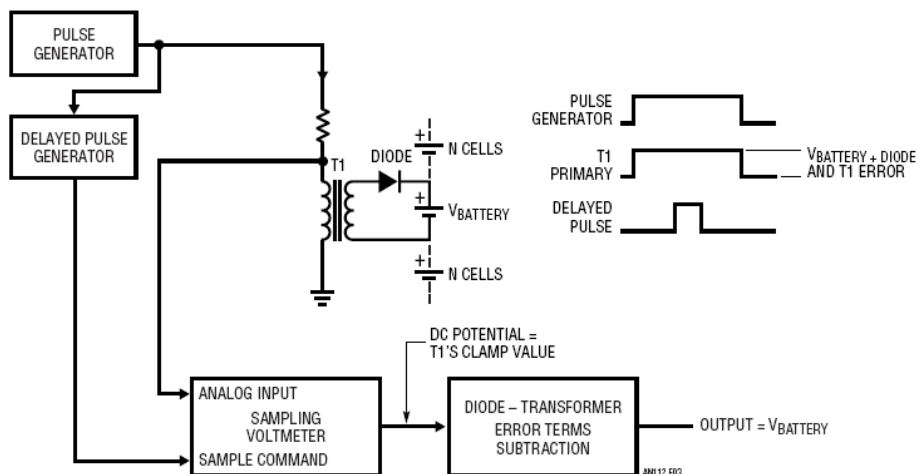


Figure 8. A transformer based voltmeter. The pulse generator will create a voltage which will be clamped (at T1) to the same voltage as the cells plus the forward voltage drop over the diode. This voltage is then forwarded to an ADC¹ in a micro controller.

¹ Analog to digital converter

Using differential amplifiers

The concept used for measuring the cell voltages in this project are ordinary differential amplifiers. High common mode voltage is not a problem since each module has its own ground reference. This implies that the highest voltage available on one module is the sum of the two cell voltages.

In the type of lithium ion batteries used in this project, the cell voltage varies between 2.5 V and 4.25 V. The optimal accuracy can be obtained if this range could be offset and scaled to the range 0 V to 5 V which is the operating range of the ADC in the micro controller. This offset and gain can be accomplished with a differential amplifier shown in Figure 9. If the desired measuring range is 2.5 V to 4.35 V the following equation is wanted in the case of measuring the second cell. (Similar equation holds for the first cell.)

The voltage to measure has a span of $4.35 - 2.5 = 1.85$ V. For best resolution this range should be scaled to 5 V and thus it has to be multiplied with 2.7. If 2.5 V is subtracted the ADC input voltage will range from 0 to 5 V.

$$V_{out} = (V_2 - V_1 - 2.5) \cdot 2.7$$

Formula 1

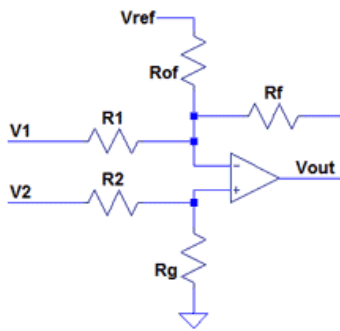


Figure 9. An operational amplifier connected as a differential amplifier. V1 is the voltage over the first cell and V2 is the sum of the voltages over the first and the second cell.

If the operational amplifier, OP Amp, works in its active region, the following holds:

$$V_+ = V_-$$

Formula 2

Positive OP Amp terminal – Voltage division:

$$V_+ = V_2 \cdot \frac{R_g}{R_g + R_2}$$

Formula 3

Negative OP Amp terminal – Kirchhoff's law:

$$\frac{V_- - V_1}{R_1} + \frac{V_- - V_{ref}}{R_{of}} + \frac{V_- - V_{out}}{R_f} = 0$$

Formula 4

Solving the equation system (formulas 2, 3 and 4) and identifying the terms with Formula 1, the following values are obtained if both R_1 and R_2 are chosen equally to 10 k Ω :

$$\begin{aligned} R_1 &= 10 \text{ k}\Omega \\ R_2 &= 10 \text{ k}\Omega \\ R_g &= 10 \text{ k}\Omega/\text{k}\Omega \\ R_f &= 27 \text{ k}\Omega \\ R_{of} &= 10 \text{ k}\Omega \\ V_{ref} &= 2,5 \text{ V} \end{aligned}$$

Formula 5

Measuring the balancing current.

There are mainly two alternatives to choose from when measuring current. The first is to use the same principle as a current clamp meter, namely the Hall effect named after Edwin Hall who discovered the effect in 1879. The method senses the magnetic field that is created around a wire when current flows through it. This method is suitable for all kinds of current ranges and does not involve any extra resistance in the wire which in turn results in negligible losses. The downside is that it is much more expensive compared to the alternative described below. It also takes a large physical form due to the ferrite core that surrounds the wire.

A cheaper method is to use a series resistor and then measure the voltage over the resistor when current flows through it, Ohm's law. The resistor is often referred to as a shunt resistor and can be in the range from 1 m Ω up to 100 m Ω depending on the magnitude of the current, the effect that can be dissipated and the accuracy required. If a small resistor is used it is probable that the voltage over it needs to be amplified before being fed to an ADC. This can be accomplished by using a differential amplifier connected as in Figure 10.

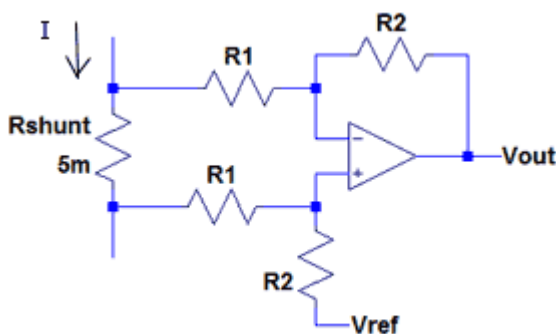


Figure 10. A differential amplifier used to measure current through Rshunt. The output voltage, Vout, can be scaled and offset by changing the values of R1, R2 and Vref. The gain is set by the quota of R2 and R1 and the offset is set by Vref.

The result from the ADC is stored in a ten-bit register. That means that the input voltage 0 - 5 V corresponds to the register values 0 - 1023. To simplify the software it is desirable

that, for example, a current increase of 1 A result in a register value increase of 100. This gives a resolution of 10 mA and a measuring range of 10.23 A.

If measuring both positive and negative currents, an offset reference voltage, V_{ref} , must be inserted to make a current of 0 A result in, for example, half the maximum output voltage.

If the gain of the differential amplifier is 97.6 ($R2/R1 = 97.6$) the result will become close to the desired;

$$V_{Rshunt} = I \cdot 5\text{m}\Omega$$

$$V_{out} = V_{Rshunt} \cdot \frac{R2}{R1} + V_{ref} \quad \text{Formulas 6a, 6b, 6c}$$

$$ADCregister = V_{out} \cdot \frac{1023}{5\text{V}}$$

If choosing $R1$ to $1\text{ k}\Omega$, $R2$ to $97.6\text{ k}\Omega$ and V_{ref} to 2.5 V the result in the A/D converter register will be

$$ADCregister = I \cdot 5\text{m}\Omega \cdot \frac{97,6\text{k}\Omega}{1\text{k}\Omega} \cdot \frac{1023}{5\text{V}} + 2,5\text{V} \cdot \frac{1023}{5\text{V}}$$

$$ADCregister = \frac{I}{\text{A}} \cdot 99,84 + 512$$

Formulas 7a, 7b, 7c

$$ADCregister \approx 100 \frac{I}{\text{A}} + 512$$

Driving transistors

In this project, MOSFETs² are used as electronically controllable switches. These transistors are different from the BJTs³ since the current is controlled by the voltage applied at the gate of the MOSFET and not by the current flowing into the base as in the case of using BJTs. MOSFETs are the primary choice when it comes to switching applications.

The gate of the MOSFET can be thought of as a capacitor that needs to be charged very quickly. But the faster the gate needs to be charged, the bigger current needs to be applied. There are special IC⁴ called drivers used for this application. They are capable of delivering a big current (up to 1.5 A) for a short period of time. The IC used in this project is called TC4428 and it has two channels where one is inverted and the other is non-inverted. Its functional block diagram is shown below in Figure 11. The inverted signal is used for driving the P-type MOSFET and the non-inverted signal is used for the N-type MOSFET.

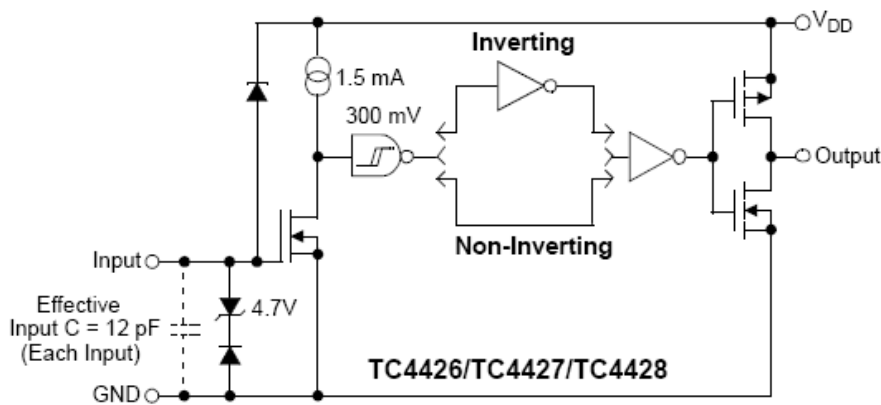


Figure 11. The functional block diagram of a dual 1.5 A MOSFET driver. The input is connected to the micro controller and the output to the gate of the transistor via a resistance to limit the current.

Communication with other modules

To report the cell voltages, balancing current and temperature or to start balancing at a given signal, the modules have to be able to communicate with other modules or a master card. This can be done by using the CAN⁵ bus. CAN uses a two wire cable where one signal is non-inverted and the other is inverted (called CAN-high and CAN-low). This greatly improves the speed and reliability of the bus, even if used in application with high EMI⁶.

Since all modules have different ground potentials, there has to be some kind of digital isolation between the micro controller and the CAN IC. For this application, Analog

² Metal–oxide–semiconductor field-effect transistor

³ Bipolar junction transistor

⁴ Integrated circuits

⁵ Controller area network

⁶ Electromagnetic interference

Devices has come up with a digital isolator called ADUM1201 which uses the iCoupler® technology. The technology uses a combination of transistors and transformers and is superior to other methods such as optocouplers in the sense of power consumption, speed and linearity (10). The block diagram is shown below in Figure 12.

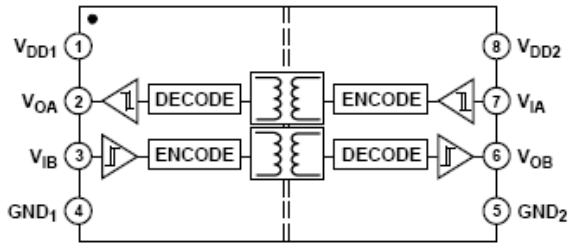


Figure 12. The block diagram of the digital isolator ADuM1201 from Analog Devices.

For testing and evaluation purposes the PC program CANalyzer from Vector has been used to monitor the CAN messages.

CANalyzer allows the user to display the data in physical units and to show graphs of how the values change with time. A screenshot from the program is shown in Figure 13.

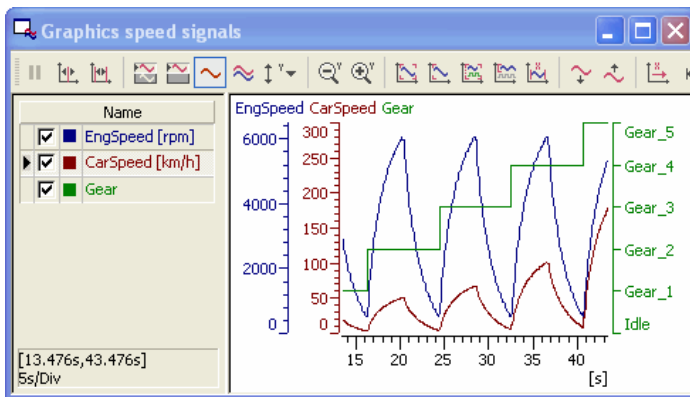


Figure 13. A screenshot of the graph-functionality in CANalyzer.

The tool has been very handy throughout this project and allows a well structured monitoring of the cell voltages, currents and temperatures.

Evaluation

Two versions of the card have been constructed in this project. The first version was used for testing and evaluating the concept, to find faults and things that could be improved. The second version is the one that has been produced in ten copies.

Most of the made tests were performed on both versions and a comparison can be presented, but in some cases, it has only been performed on the first version. The following chapter will present the results from the tests made mainly from the second version, but also from the first if they are very different or interesting.

Measuring voltages

In theory

When using the modular approach, and thus using only differential amplifiers to measure the voltage, it makes the task simple. The use of rail-to-rail output OP Amps makes it possible to use the whole output range (0-5 V) and thus achieving high accuracy. An increase in the ADC⁷ register value with one unit will correspond to a cell voltage increase of about 2 mV according to formula 1 (page 15) and formula 6c (page 17).

To calculate the cell voltage at a given ADC value, the following formula, formula 8, can be used and will result in the voltage given in mV. This formula is theoretical and builds on the above mentioned equations.

$$V = (1,81 \cdot ADCvalue + 2500)mV \quad \text{Formula 8}$$

The ADC register values at different cell voltages are shown in Table 2.

Table 2. The table shows which value in the ADC register that corresponds to a specific cell voltage. The Vout voltage refers to Figure 9.

Cell Voltage [V]	Vout [V]	ADC register value
2,50	0,00	0
3,00	1,35	276
3,50	2,70	552
4,00	4,05	829
4,35	5,00	1023

⁷ Analog to Digital Converter

In practice

The voltage of the cell was simulated using a voltage supply and while changing the voltage, the ADC result was noted. The results are plotted in Chart 1. The results from both voltage measuring circuits (V1 and V2) are very similar why only the measurements for V2 are showed.

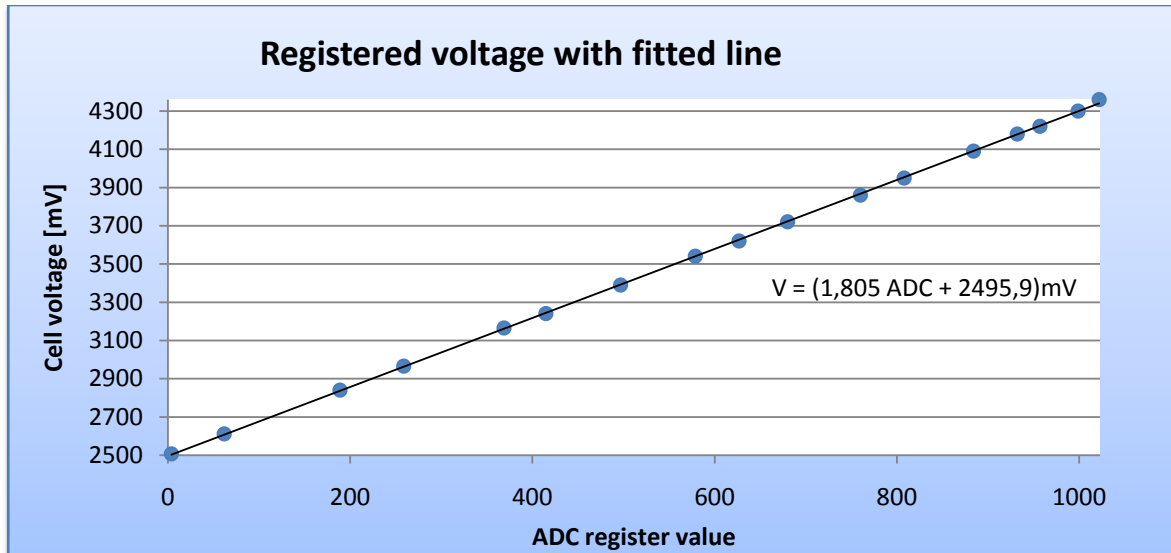


Chart 1. The noted ADC register values at given cell voltages simulated with a voltage supply.

The result is very linear and a good approximated linear equation can be used to calculate the voltage at a given ADC register value. The difference compared to the theoretical equation is mainly because of the tolerance in the resistors used in the differential amplifier. The error statistics when using the equation for the line compared to the actual voltage is shown in Table 3.

A separate calibration as described above has been made for both voltage measuring circuits on all nine modules. This means that 18 different equations are used depending on which card and voltage measuring circuit that is used.

The chosen equation depends on the ID of the card. Information about how to set the card ID is found in the chapter about CAN later in this report.

Table 3. Statistics of the errors when using the fitted line equation compared to the actual voltage. The statistics are based on all nine cards.

max error	5 mV
min error	-8 mV
Average error	-1 mV
Standard deviation	3 mV

The influence of current flow

The series resistance of the batteries used in this project can be estimated to about 7 m Ω according to Appendix 1. I have also discovered that there is a chemical process in the battery that increases the voltage when current has been flowing in to the battery for a long period of time. The effect of the chemical process is small; its influence over time can be seen in Chart 2.

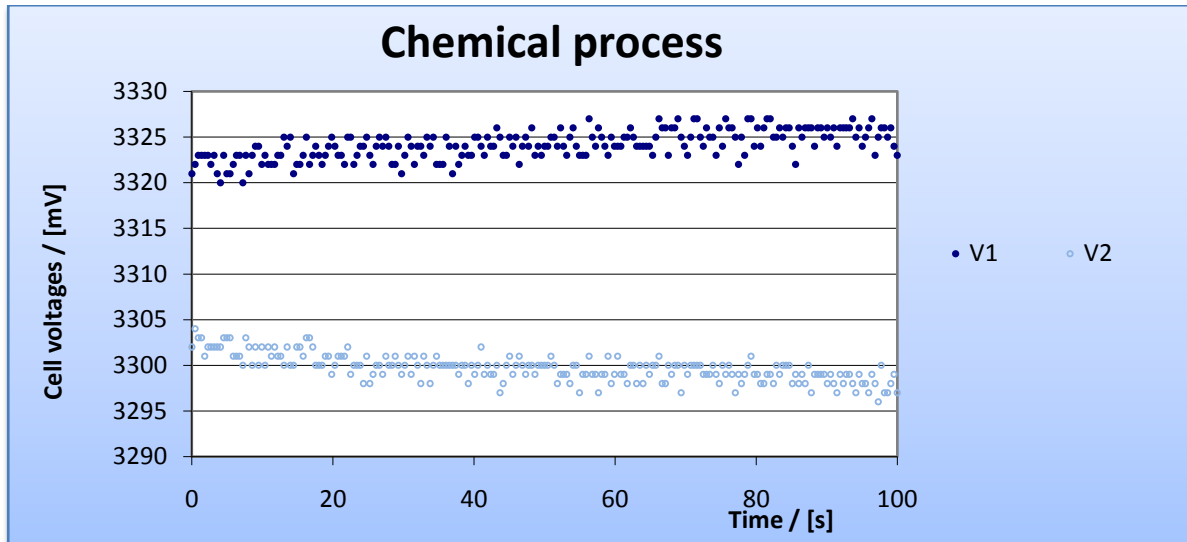


Chart 2. The effect of the chemical process. The chart shows the measured voltage of both cells after a balancing current of 3.5 A was just switched off. It varies in average about 5-10 mV.

When balancing current flows through the card, there will be a voltage drop over copper tracks, fuses and transistors which will tend to make the voltage of the cell look higher or lower depending on which way the current flows as shown in Chart 3.

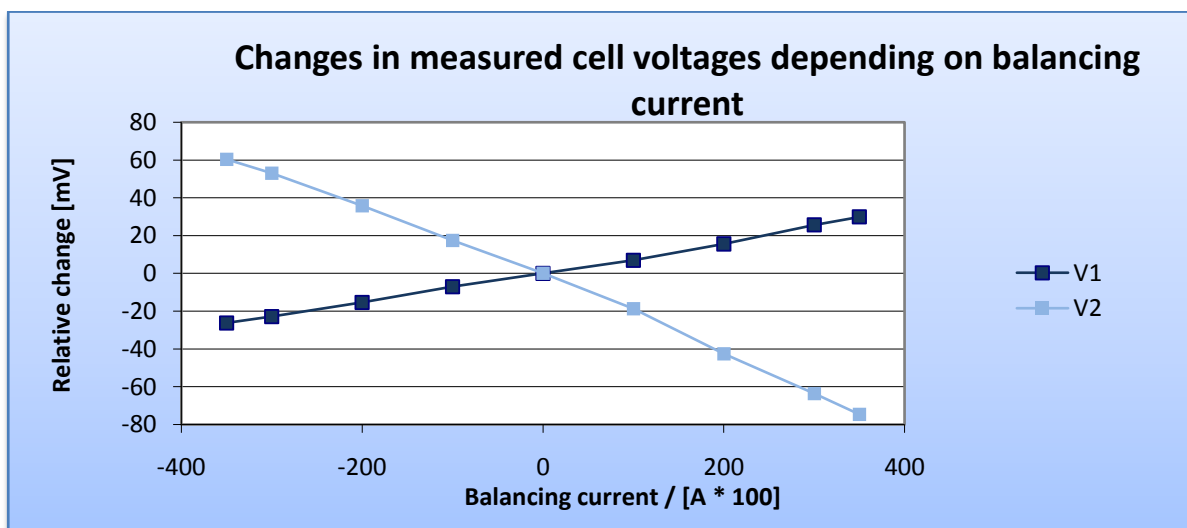
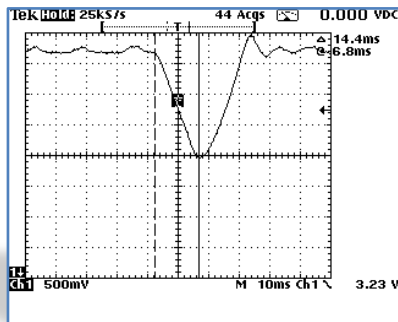


Chart 3. The change in measured cell voltage due to the resistance on the cards, depending on the balancing current.

To get an accurate cell voltage reading no balancing current should flow through the card. For this reason the software has been designed so that every fifth second, the balancing current is shut down for a couple of milliseconds and during that break, the voltage is measured. The current as a function of time at this break is shown in Oscilloscope copy 1. The horizontal lines represent about 1 A each. The balancing current here is 3.5 A. When the current has reached zero (or more correct, after 15 ms), the battery voltage is sampled.



Oscilloscope copy 1. The current at the time of the voltage measurement break.

When using this method of sensing the battery voltage, a variable that holds the correct voltage, independent of the balancing current, can be implemented using the above method. Chart 4 shows the result from an experiment where the value of the variable and the original voltage was recorded during different balancing currents. For each step in the chart, the balancing current was changed to 1, 2, 3, 3.5 and then back to 0 A with about 25 seconds at each value. At the balancing current 3.5 A it is possible to see a slight increase in the filtered signal. This might be because of the chemical process described earlier.

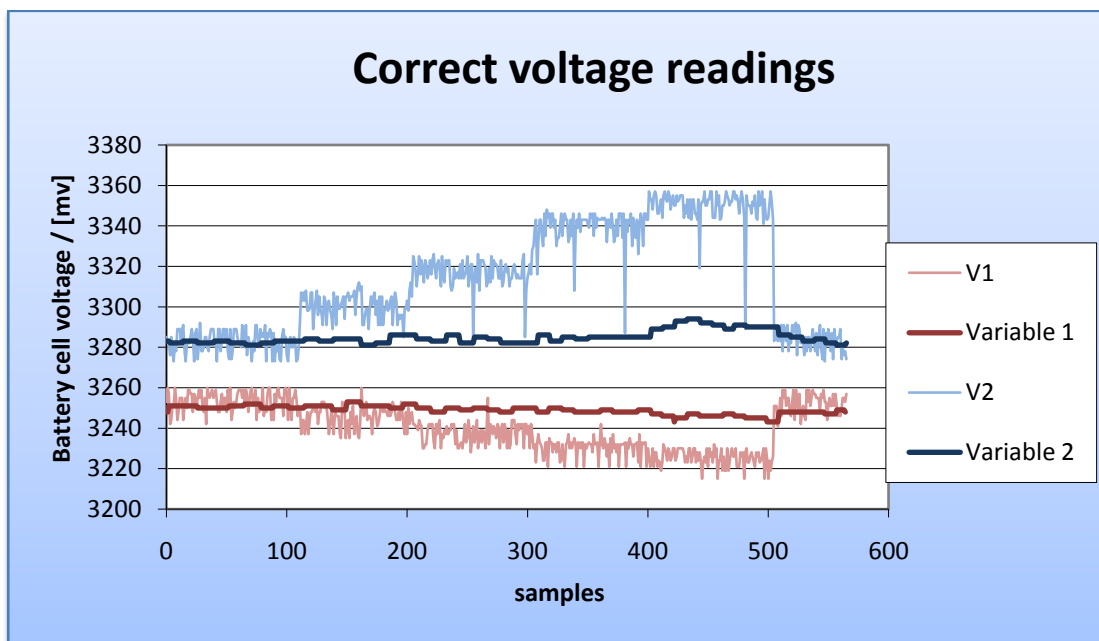


Chart 4. The chart shows that it is possible to minimize the influence of balancing current flow when measuring cell voltages.

Measuring balancing current

The balancing current is also registered by the micro controller via an ADC. The current is measured using a shunt resistor as described on page 16.

An instrumentation amplifier is a kind of differential amplifier that has a very high common mode rejection ratio. It should be used in cases where the common mode voltage varies a lot with time. In this project the common mode voltage will be almost equal to the voltage of the first cell and therefore the need for an instrumentation amplifier is not necessary. An ordinary, single OP Amp connected as a differential amplifier can be used.

In theory

According to formula 7, the relation between balancing current and the ADC result register is described with the following equation.

$$ADC_{register} \approx 100 \cdot \frac{I}{A} + 512 \quad \text{Formula 9}$$

In practice

The reality usually differs from the theory, but the current measurement has proven to be very close to the theory. The reason for this might be the use of 0.1%, 97.6 kΩ resistors for the differential amplifier. The result from a measurement where the current has been adjusted to specific values and the ADC register value noted is shown in Chart 5. In the software, the current is saved in the unit 0.01 A to increase accuracy. This means that the formula used can be simplified to

$$ADC_{register} = \frac{I}{0.01A} + 512 \quad \text{Formula 10}$$

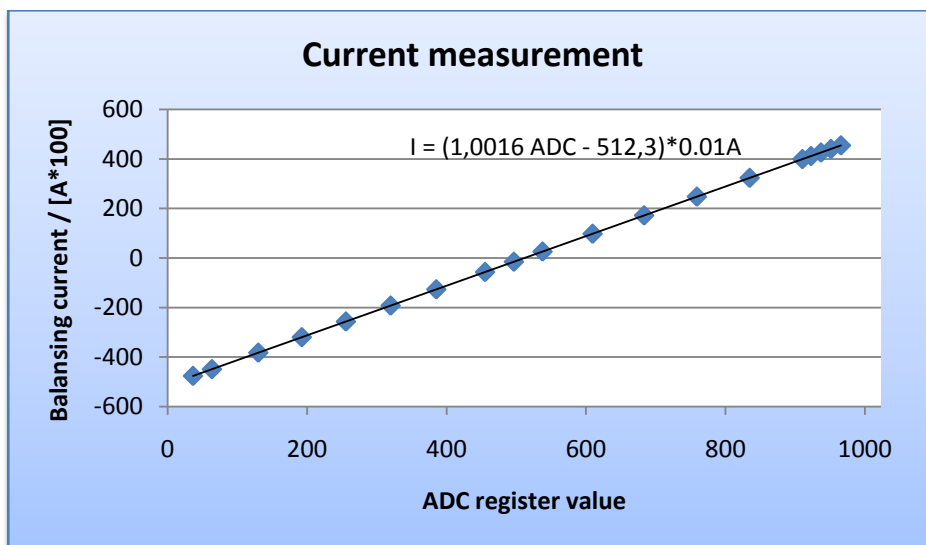
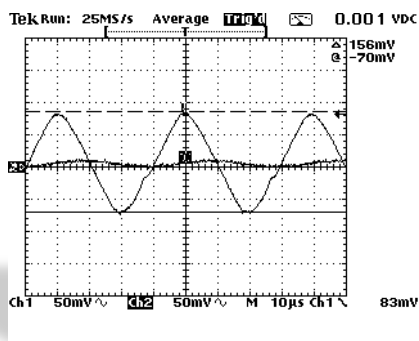


Chart 5. The results from a current measuring experiment. The chart shows that the linear approximation is very close to the theoretical values.

Since the accuracy of the current measurement is not critical for this application, I have decided to use this equation for all cards without any further investigation of the differences between the cards.

Depending on the switch frequency and the inductance of the inductor, the current ripple will vary. The recognized maximum current ripple is usually one tenth of the maximum current (3). In this project the switch frequency is 25 kHz and the inductance is 120 μ H. This implies that the current will increase through the inductor during 20 μ s and decrease during 20 μ s, if the duty cycle is 50 % and the battery cells have the same voltage. This has been investigated and the measurement is shown in Oscilloscope copy 2.

In Oscilloscope copy 2 there are two graphs. Both show the current, but they have different low pass RC⁸ filters. The first filter has a cutoff frequency of 160 kHz, removing only high frequent noise and the second filter returns the average current due to its cutoff frequency of 1.6 kHz. The two signals are both fed to separate ADC channels of the micro controller.



Oscilloscope copy 2. The current ripple as it is seen by the ADC when both cell voltages are the same and the duty cycle is 50%. The voltage has a dc value of 2.5 V and the ripple is 156 mV peak-to-peak. That corresponds to a current ripple of 320 mA peak-to-peak.

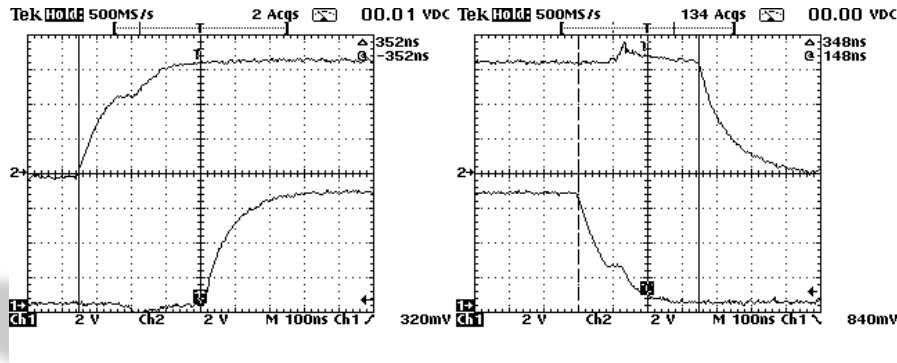
Driving transistors

For this project I have used a micro controller from Renesas called R8C23. This controller has a nice feature when it comes to driving transistors. More information about the controller will be described at the software part of this report. For now, it can be said that it is possible to generate a complementary PWM-signal where the dead time can be controlled.

⁸ Resistor-capacitor

Dead time

Dead time means the time where none of the transistors are activated. Since it takes a while for the transistor to stop conducting when the gate is discharged, the controller has to wait a while until the other transistor is turned on. The dead time depends on the size of the gate capacitance, the series resistances and the applied charge voltage. Measurements of the gate voltages have been performed on the card and the results are shown in Oscilloscope copy 3.



Oscilloscope copy 3. Measurements of the dead time. The P-type MOSFET is the upper graph and the N-type is the lower graph. The P-type MOSFET will stop conducting when the gate voltage becomes high and the N-type MOSFET will stop conducting when the gate voltage becomes low.

The R8C23 allows the programmer to change the dead time in steps of one clock cycle which is 50 ns. The dead time was chosen to $7 \times 50 \text{ ns} = 350 \text{ ns}$ based on the results in Oscilloscope copy 3.

Gate resistances.

There are mainly two things that have to be considered when choosing the series resistances between the driver and the gate of the MOSFET, called gate resistance. The lower the resistance, the faster the gate will charge, the less dead time it will be and lower switch losses will arise in the transistor. But the resistance must not be too low due to the maximum current the driver can deliver. A too low value might also cause the transistors to reach self oscillation.

In this project, the gates will be charged to a maximum of 8.5 V. If the maximum current is 1.5 A this means that the lowest value of the gate resistance, for the maximum current reason, is about 6Ω (disregarding the on-resistance of the transistors in the driver). This value is low and the transistors might start to oscillate. Therefore, 47Ω was chosen for the gate resistance to be safe and this seems to work nicely.

Temperature measurement

Two different circuits have been used to measure the temperature of the card/battery terminal.

The first method was used on the first version of the card and utilized an IC for temperature measurement. The IC was called DS60 and gave out a voltage that was proportional to the temperature according to Figure 14.

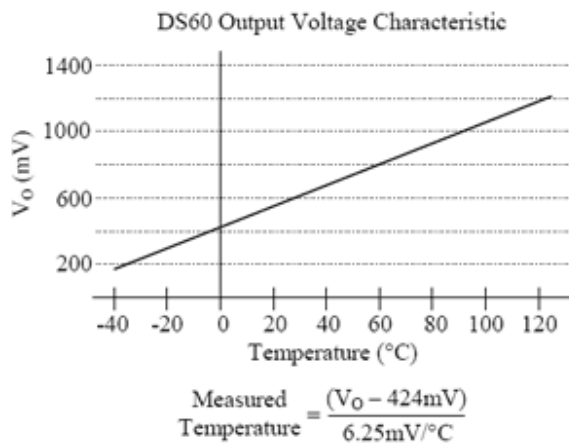


Figure 14. The output voltage of the temperature sensor DS60.

The IC worked well, but the accuracy was not very good since the output voltage only reached from 0.2 to 1.2 V, not using the whole range of the ADC. The price of the DS60 was about 8 SEK which is expensive compare to a NTC⁹-thermistor with a cost of only 5 % of that value.

The thermistor is a better choice regarding the space taken on the board and the accuracy obtained. The thermistor is connected to the ADC according to Figure 15.

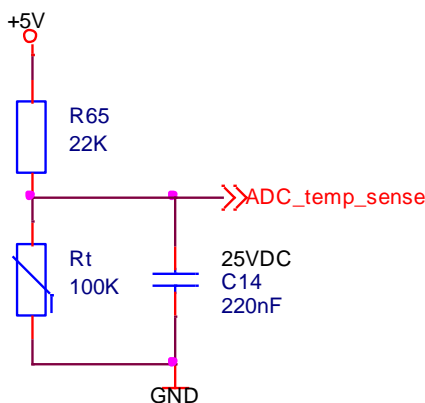


Figure 15. The connection of the thermistor, R_t , to the ADC.

⁹ Negative Temperature Coefficient

The circuit will result in the temperature-voltage dependency shown in Chart 6.

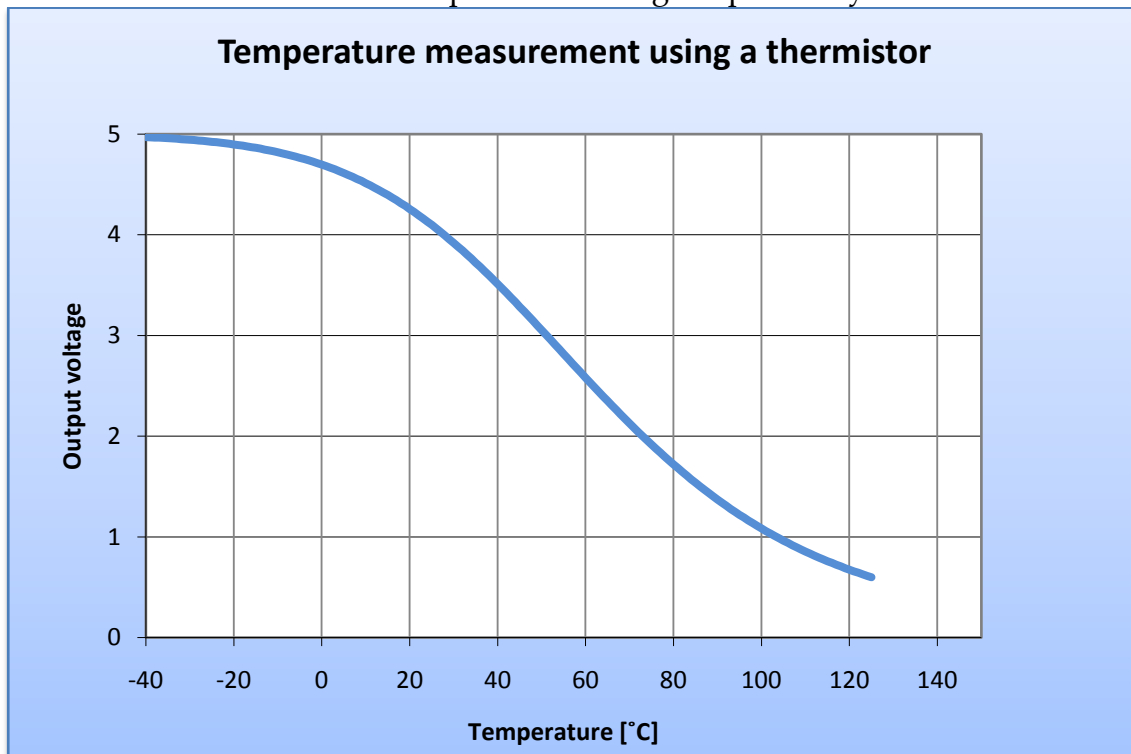


Chart 6. Temperature measurement using a thermistor in a circuit like Figure 15.

This method uses the whole range of the ADC and has also different resolutions at different temperature ranges. As can be seen in the chart, the highest resolution (the steepest slope) is in the range from 40°C to 80°C which is suitable for this application. At this range, a decrease of one ADC register value corresponds to a temperature rise of 0.1°C. The accuracy is about 5% with respect to the tolerances of the thermistor and the resistor.

The capacitor, C14, in Figure 15 was added to implement a low pass filter with a cutoff frequency of about 30 Hz to remove noise.

A technique called linear interpolation has been utilized to quickly calculate the temperature that corresponds to a specific ADC value. More information about this is available in the software part of this report.

Protection

Over current

In case of failure to drive the transistors which might be a result from a hardware or software error, it is important to implement protection against over current. A software protection might fail if the programmer makes a mistake. Therefore, it is also necessary to have a hardware protection that shuts off the transistor if the balancing current gets too high independent of the program code.

Refer to Appendix 2 for the circuit diagram. The output from the current measuring circuit, V_{curr} , is usually at 2.5 V when no balancing current flows. This voltage will change to 4.95 V and 0.05 V when 5 A and -5 A flows, respectively.

V_{curr} is forwarded to two comparators via a voltage divider (due to that the maximum common mode voltage input of the comparators is $V_{cc}-1.5V = 3.5V$). This voltage is then compared with the voltages 0.034 V and 3.41 V. If the voltage goes outside this range, one of the comparators, IC21D or IC21E, will pull down the open collector output and the *overcurrent*-signal will signal to the micro controller that an over current event has occurred.

The micro controller has a built in hardware protection feature which will disable the transistor outputs if the *overcurrent* goes low. This feature has been tested and it works very well. Details about this feature can be found later in this report in the *Pulse Output Forced Cutoff* chapter.

As an extra protection the second version of the card also has a 12 A super fast fuse at the terminal of each battery cell.

Over voltage

Refer to Appendix 3 for the circuit diagram. The battery cells are meant to operate between 2.5 V and 4.25V to not reduce their lifetime. This balancing system cannot disconnect a battery cell from the stack to protect it, it can only signal error messages over the CAN bus when the voltage gets too high or too low. To protect the circuits from erroneous connections and high voltage, a hardware voltage monitoring system has been designed. If the voltage goes above 4.31 V or below 2.5 V the protection system will shut down the onboard voltage regulator and thus also the micro controller and put on a red LED¹⁰ to indicate voltage error. The controller board will detect that a card has disappeared from the CAN bus and will immediately turn off the charging or discharging of the battery cell stack. This system works as a redundant protection system in case the ADC, which measures the cell voltages, does not work as anticipated due to a hardware error, for example.

This protection system must not rely on that the onboard 5 V regulator works. Therefore, the reference voltage has to be created directly from the available voltages from the two battery cells. This cannot be done using only resistors as a voltage division since the battery cell voltages change over time. Instead, a reference diode has been used for this purpose.

The TL431 is a programmable reference diode. Its functional block diagram is shown in Figure 16. It works by adjusting the voltage at its cathode, so that the voltage at its reference terminal will become 2.5 V. The cathode voltage, V_{KA} , can thus be programmed with the two resistors, R1 and R2.

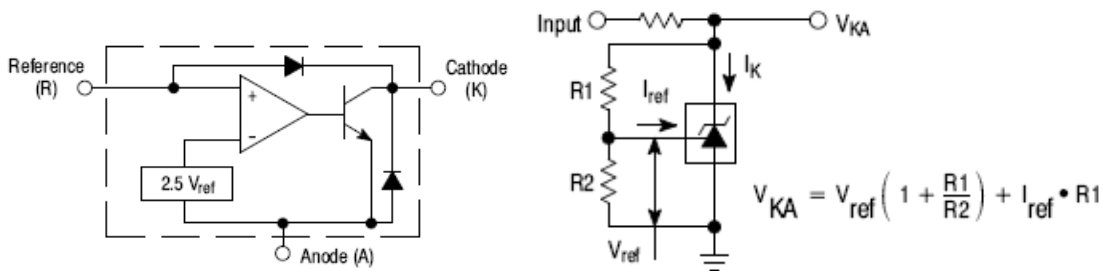


Figure 16. To the left, the functional block diagram of the TL341 reference diode. To the right, the connection for using the TL341 as a programmable voltage reference.

By choosing the combination $R1=22 \text{ k}\Omega$ and $R2 = 30 \text{ k}\Omega$, V_{KA} will equal 4.36 V in theory. This combination was chosen because then the voltage comparator, IC21c, activated the output at $V1=4.31$ and resets when $V1$ went down to 4.26 V.

This combination of $R1$ and $R2$ gave the closest and higher value compared to 4.25 V where the comparator output was deactivated, including hysteresis.

¹⁰ Light Emitting Diode

The micro controller, R8C23

When deciding which micro controller to use for this project there were some requirements that needed to be satisfied.

The first was that the controller needed a CAN module to be able to communicate with the surroundings. The second was the ability to generate a PWM signal, preferable of complementary type with dead time. Third, it had to be fast enough to sample the current and adjust the transistor outputs. Fourth, it would be more convenient and easier to program if Aros had it in stock and if there was a bootloader software available that Aros had used earlier.

It came down to two available controllers to choose from. R8C32 or M16C29

Some simulations were performed in the free program Switcher CAD III from Linear Technology that is based upon a SPICE engine. If one of the transistors was interchanged with a short circuit, the inductor would become exposed to the voltage of one cell and the inductor current would start to rise. The question was how much time it would take for the current to reach the saturation current of the inductor (~ 5 A). The result from the simulations shows that it takes approximately of $150\text{ }\mu\text{s}$ if a $100\text{ }\mu\text{H}$ inductance is used.

The ADC conversion time of both controllers was $3.3\text{ }\mu\text{s}$. With that in mind the decision was taken to use a $100\text{ }\mu\text{H}$ inductor and the R8C23 micro controller due to its simpler architecture and that the M16C29 was over qualified for the tasks required.

The R8C23 is an 8-bit micro controller in a LQFP48¹¹ as shown in Figure 17. This controller has many features and is very suitable for this project. It was chosen because it had all the required functionality such as CAN, complementary PWM and many ADC channels, but also because Aros had it in their stock. Here are some of the features listed.



Figure 17. A LQFP48.

- 8-bit Multifunction Timer with 8-bit prescaler (Timer RA and RB): 2 channels
- Input Capture/Output Compare Timer (Timer RD): 16-bit x 2 channels
- Timer with compare match function (Timer RE): 1 channel
- UART/Clock Synchronous Serial Interface: 1 channel
- I²C-bus Interface TWI: 1 channel
- LIN Module: 1 channel
- CAN Module (2.0B): 1 channel, 16 slots
- 10-bit A/D Converter: 12 channels
- Watchdog Timer
- Clock Generation Circuits. External clock up to 20 MHz
- Voltage Detection Circuit

¹¹ Low-profile Quad Flat Package, 48 pins

- Power-On Reset Circuit
- I/O Ports: 41
- External Interrupt Pins: 8
- Data Flash: 2KB

Complementary pulse width modulation, PWM

The R8C23 has a great feature when it comes to driving transistors in complementary mode, especially for three phase motor controllers.

In Figure 18, the output model for complementary PWM mode is shown. The registers TRD0 and TRD1 hold the value of the timer counters. The offset between them will control the dead time. The duty cycle of the three complementary output pairs B0/D0, A1/C1 and B1/D1 can be controlled individually by modifying registers TRDGRB0, TRDGRA1, TRDGRB1, respectively. The PWM period, in timer clock cycles, is set by the TRDGRA0 register and the offset between TRD0 and TRD1.

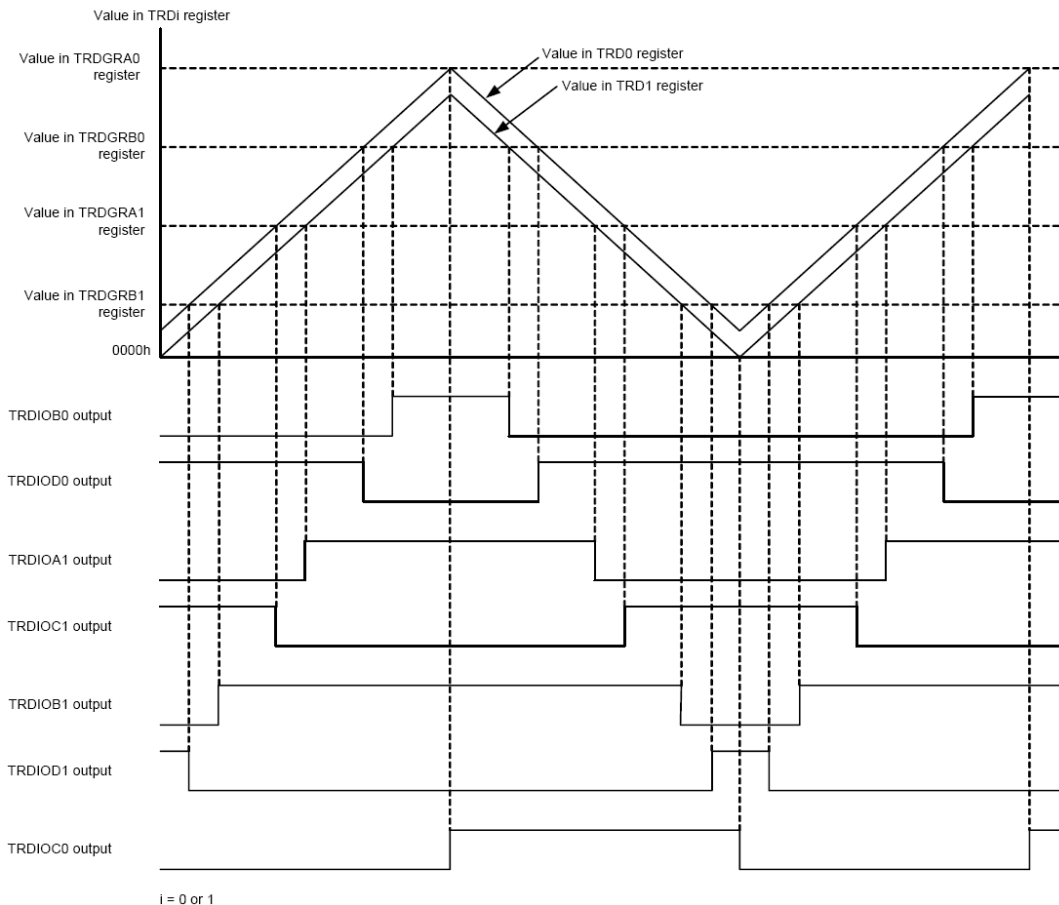


Figure 18. Output model of the R8C23 controller for complementary PWM mode

In this project, the output pair B0/D0 has been forwarded to the transistor driver. A1/C1 has been connected to two LEDs which makes it possible to fade the LEDs, if desired.

The TRDGRA0 register has been written to 400 and the offset to 7 which means that the PWM frequency became 25.32 kHz. Higher frequencies can be used to lower the current ripple, but this will also limit the resolution in controlling the voltage between the transistors and thus also the balancing current; a duty cycle of 200/400 that changes to 201/400 gives less balancing current change than a duty cycle change from 100/200 to 101/200.

Analog to digital converter, ADC

There is also another thing that limits the possibility of increasing the PWM frequency. That is the speed of the ADC. The balancing current is measured and input at an ADC channel and is sampled synchronously with the output PWM signal to the transistors.

There is a feature in the R8C23 that makes it possible to trigger the ADC sampling at the moment when the timer counter in Figure 18 is at its top-most or bottom value. This makes it possible to sample the average current according to Figure 19.

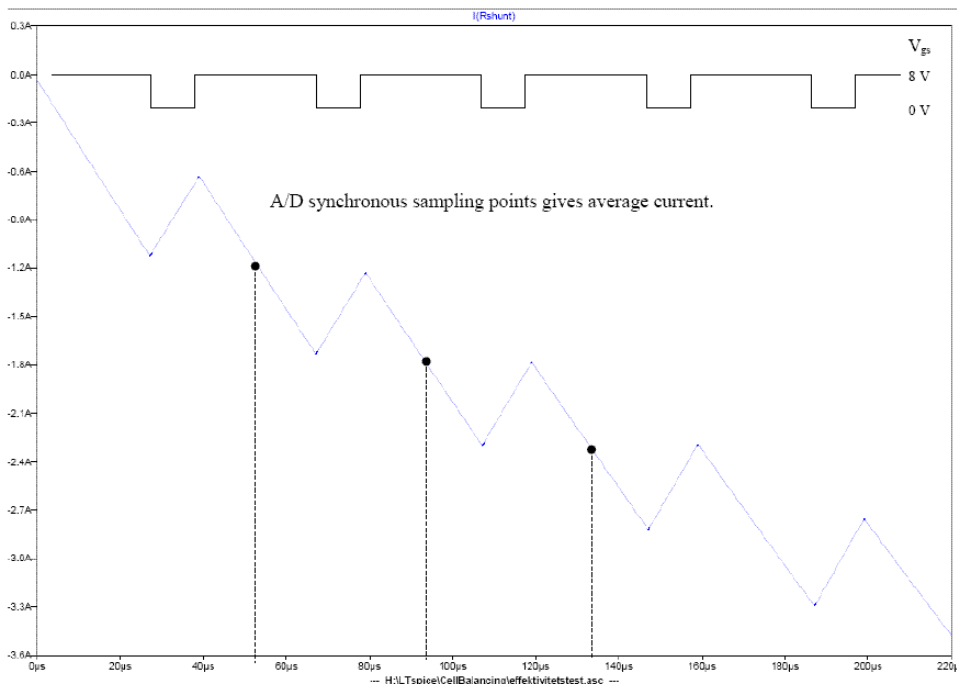
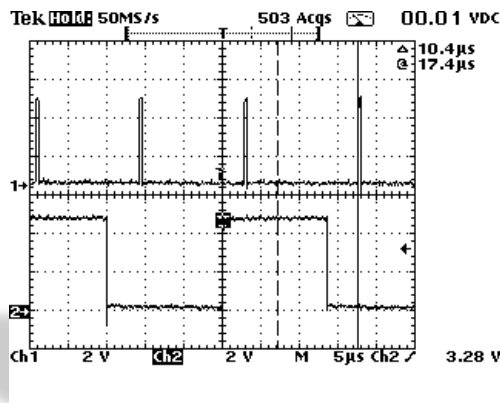


Figure 19. The upper graph shows the gate voltage of the n-type transistor. The lower graph shows the current flow through the inductor. When sampling the current at the moment where the transistor has been turned on half the time of the whole duty cycle, the average current can be read.

The current is always sampled at the top value of the timer counter. All the other ADC channels (voltages, temperature and low pass filtered balancing current) will take turns in being sampled at the bottom value. Therefore, the ADC has to be reconfigured at each interrupt to switch between the *triggering at high-mode* and the *triggering at low-mode*. This takes time and if the PWM period is too short the ADC will not have enough time to reconfigure and will thus skip every other occasion.

A test has been made and the result is that a PWM frequency of 33 kHz is just at the limit before the ADC starts to skip every other occasion. Therefore, 25 kHz was chosen to be safe. Oscilloscope copy 4 shows where the ADC interrupt occurs compared to the transistor output, B0. It can be seen that it takes about 10.4 μs between the sampling starts and the execution of the ADC interrupt routine.



Oscilloscope copy 4. The upper graph shows when the ADC interrupt routine is executed. The lower shows the output from the B0 pin. Setting an output pin high or low on the micro controller takes 0.2 μs .

By performing different calculations in the ADC interrupt routine and measuring the routine execution time the test results was obtained. See Table 4.

Table 4. The table shows the result from a test that was made to find out how long the maximum execution time of the ADC interrupt routine could be at 33 kHz before it started to skip every other interrupt. The header frequencies refer to the PWM frequency.

Execution time	33 kHz	25 kHz
4.5 μs	OK	OK
7.0 μs	OK	OK
7.8 μs	Not OK	OK

The decision to use a PWM frequency of 25 kHz resulted in that the ADC interrupt routine would be executed every 20 μs and thus taking up much of the available processor time.

Pulse Output Forced Cutoff

The *pulse output forced cutoff* feature of the R8C23 comes in handy when an over current protection system is to be utilized. When the feature is activated it is only controlled by hardware inside the micro controller. This makes sure that the feature will work even if the programmer makes a mistake resulting in an endless loop or similar. The function is simple. It disables all complementary PWM outputs shown in Figure 18 if the input signal at the INT0-input pin becomes low. The INT0 input has a hardware digital filter and must be low for three consecutive clock cycles before a signal change is acknowledged.

Software

Programming

The program code has been written in the C language using an ordinary text editor. The code was compiled with the NC30 C-compiler and downloaded to the micro controller flash memory using an RS232 interface.

Staff at Aros have developed a bootloader which makes it possible to download the software via the CAN bus. This is very convenient and a must have in a project like this with nine different micro controllers. The bootloader has, of course, to be downloaded using a serial interface, but this must only be done once.

Aros operating system, ArOS

To be able to simplify the programming for the user and to enable object oriented programming in C, Aros have designed their own operative system called ArOS. Exactly how the system work is confidential information, but some things can be said about the functionality.

First of all, ArOS will link all the objects together and also create the h-files from the information that the programmer writes in the c-file. It also enables the user to send messages and function calls between objects in an efficient way.

ArOS calls two primary functions in all objects. *ExecuteFast* and *ExecuteIdle*. The fast function is called every millisecond and the idle function is executed whenever the fast function is not. This means that the OS never goes to sleep to save energy, but since the ADC interrupt routine will be executed very often and the controller has to be quick in its response, the sleeping might very well be omitted.

Floating point arithmetic

I have always heard that floating point arithmetic takes a very long time to perform in a micro controller compared to using integers, but I never understood how big the difference was.

A test was performed to investigate the differences in execution time. By putting a LED on before the calculation and then off, the execution time could be measured with an oscilloscope. The results shown in Table 5 show that calculating the cell voltage using floating point arithmetic takes about 9500 % of the time using integers. No floating point calculations are performed in the software of this project.

Table 5. A comparison in execution time between floating point and integer arithmetic.

Calculation	Execution time
$V1 = 1.81 * \{ADCregister\} + 2500$	284 μs
$V1 = 181 * \{ADCregister\} / 100 + 2500$	3.0 μs

Linear interpolation

As said before on page 28, a thermistor is used to measure the temperature. The dependency between temperature and the ADC register value is shown in Chart 7. As seen it is not possible to find a simple equation to describe the graph. Therefore, a look-up table has to be used.

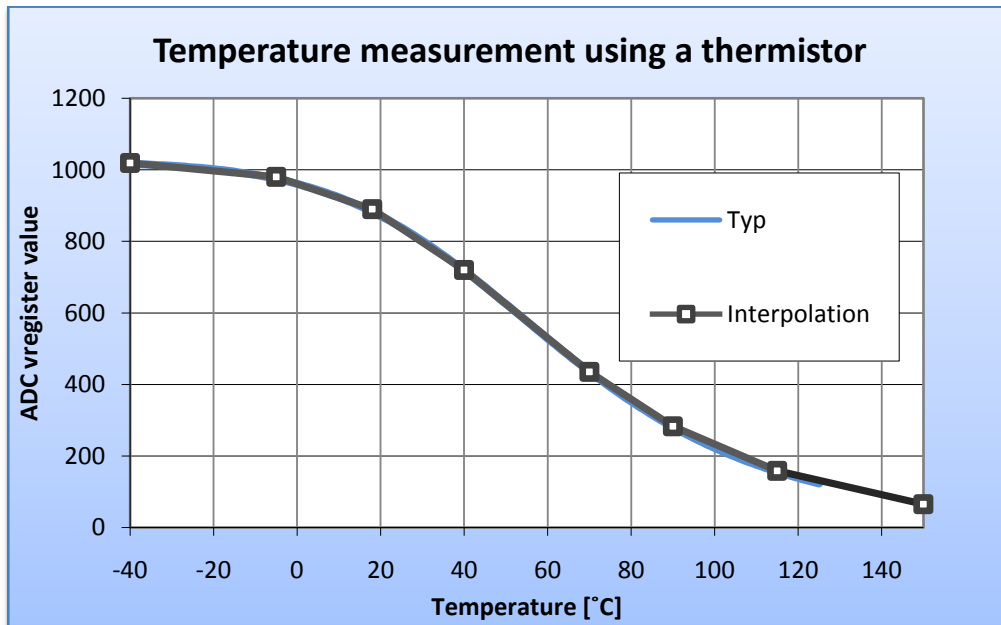


Chart 7. The ADC register value as a function of the temperature and the linear interpolation used in the project software.

Aros had previously been using a big look-up table with one ADC register value for each temperature. In the program code, the 190 numbers long look-up table was scanned from beginning until an ADC value match. The question arose if it would be faster to use linear interpolation.

Linear interpolation means that there are only a few known points (in this case, eight) and that the paths between them are approximated with a straight line. See Chart 7. To calculate an x-value (temperature) from a given y-value (ADC register) between the points (x_a, y_a) and (x_b, y_b) the following formula is used.

$$x = x_a + \frac{(x_b - x_a)}{(y_b - y_a)} (y - y_a) \quad \text{Formula 11}$$

Performed tests show that the linear interpolation method with a small look-up table is significantly faster than using a big look-up table, especially at higher temperatures as shown in Chart 8. It takes about 1.7 μs per loop iteration to go through the look-up table and about 6 μs to perform the calculations for the interpolation using Formula 11.

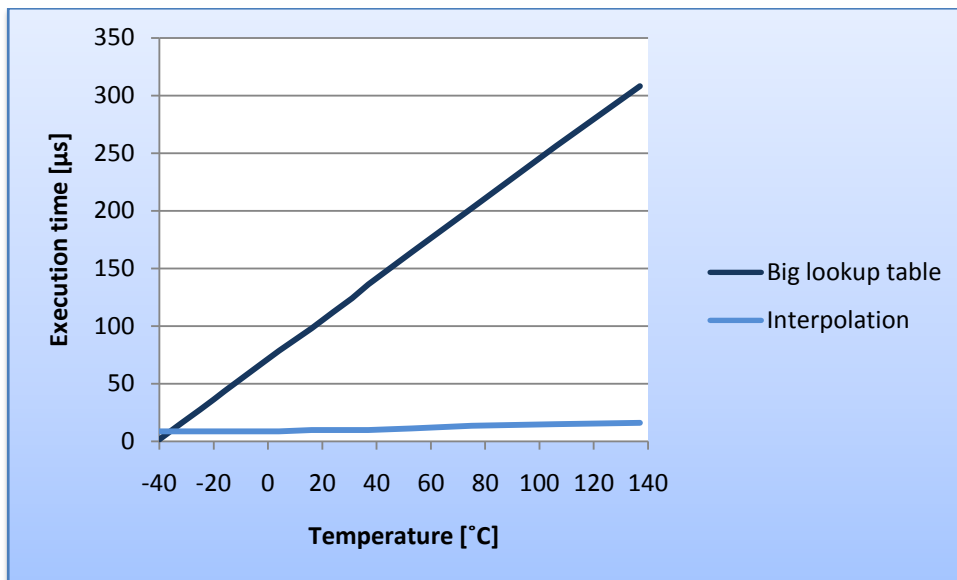


Chart 8. The chart shows the differences in execution time when linking an ADC register value to a temperature according to Chart 7.

Usually, a big lookup table is faster than other methods, but in this case, the software from Aros used a loop to scan through the table which is a slow method. There are many different algorithms to use when finding a value in a big table but more advanced methods might be hard to implement using an 8-bit micro controller.

However, the memory used by the interpolation method is only 32 byte compared to the big look-up table that uses 320 byte. The interpolation method is also very easy to adapt to other functions and is therefore a better choice.

Digital filters

It is important to get an accurate voltage reading in this project. Noise causes the input voltage of the ADC to fluctuate randomly around the correct voltage. To filter out the noise, a software digital filter has been implemented as shown in Code snippet 1.

Code snippet 1. To the left, a digital filter implementation using a time constant, TC, of eight iterations. To the right, the same filter, but with a time constant of 16 iterations.

```
filter = filter * 7 / 8 + ADC;
result = filter / 8;
```

```
filter = filter * 15 / 16 + ADC;
result = filter / 16;
```

By using powers of two as the denominator, logical shifting can be used to speed up filter calculations. When iterating the code above and keeping the value of the *filter*-variable, the filter will work as shown in Chart 9.

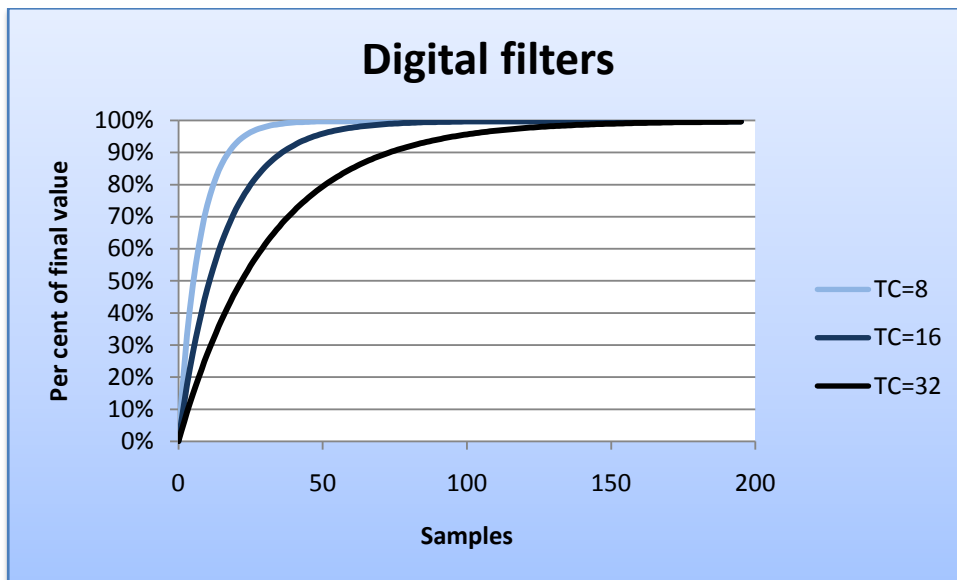


Chart 9. The chart shows the step response of three filters with different time constants, TC. It can be seen it takes 50, 100 and 200 iterations for the filter to reach their final value, respectively.

A digital filter can be seen in action in Chart 10. It works very well and the filters are used in all ADC samplings in the software of this project.

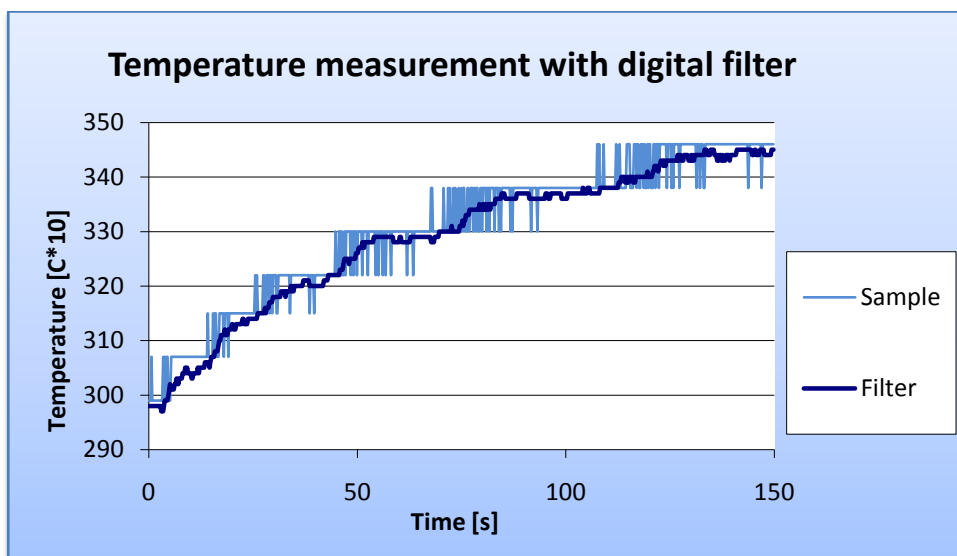


Chart 10. The chart shows the digital filter working to filter the temperature. Although the accuracy of the temperature measurement on the first card was only about 1 °C, the filter provided an accuracy of 0.1 °C.

Current regulator

After the cell voltages have been sampled and filtered, the closed loop current regulator controls the balancing current flowing through the inductance according to the scheme in Chart 11.

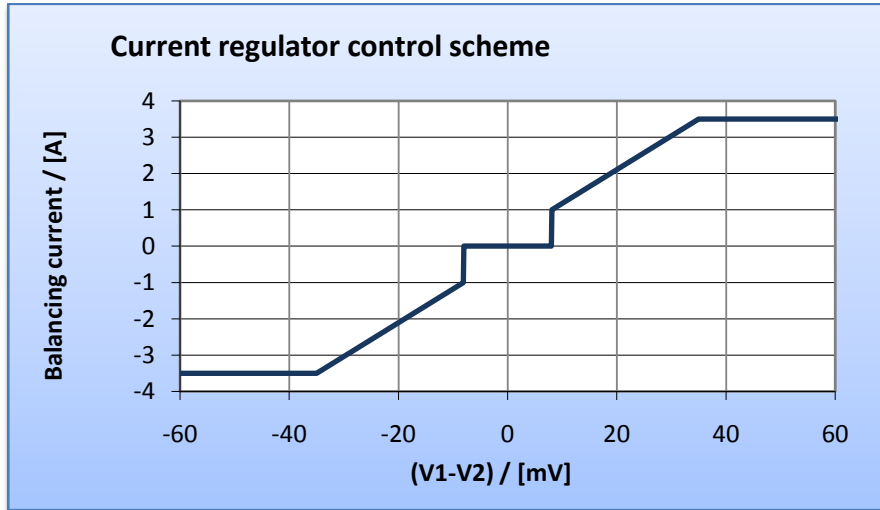


Chart 11. The chart shows how the current regulator sets the reference balancing current depending on the differences between the two cell voltages.

The current is set by controlling the duty cycle of the complementary PWM transistors. The timer period is 400 clock cycles, cc. There is major difference here between the two card versions as can be seen in Chart 12. To reach a balancing current of 4 A, the first card had to have its DC at $260/400 = 65\%$ compared to the second card with a DC at $220/400 = 55\%$. This is due to the improvements in onboard resistance which will be discussed later in this report.

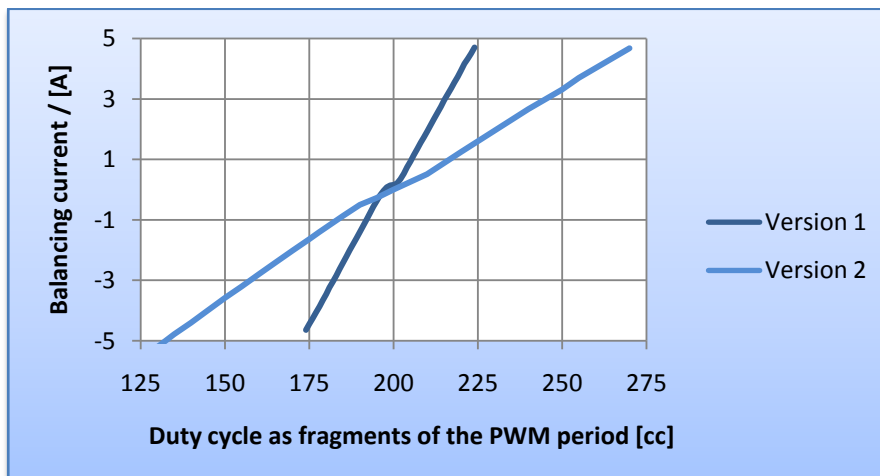


Chart 12. The chart shows which duty cycle that is necessary to regulate the balancing current to a specific value. The differences between the two versions of the cards depend on resistances in the second version. The chart is valid when the battery voltage are both 3.3 V.

Using the second version of the card, the balancing current will increase with about 200 mA for each step in duty cycle using a PWM period of 400 cc¹².

The current regulator used in this project is a very simple regulator. Though more advanced and better regulators, for instance of PI¹³-type, could have been implemented, the available free processor time is limited and a simpler solution was needed.

The chosen regulator works by comparing the actual current with the reference current. If the difference is more than 150 mA the DC is increased with one unit. If the difference is less than -150 mA the DC is decreased with one unit. This control is made every 200 μ s which is fast enough without making the regulator unstable. The regulator can change the balancing current from 0 to 3.5 A in about 14 ms. See Oscilloscope copy 1 at page 23.

CAN communication

The CAN communication was only implemented on the second version of the card. It is used to report the voltages of the two cells, the balancing current and the temperature at the cell terminal. It is also used for reporting errors to a supervising system.

The card on the first cell sends out a synchronization message so that the other cards will get the same time. The reason for this is that the cards must pause their current balancing to measure the cell voltage at the same time. Refer to *The influence of current flow* at page 22. If the cards are not synchronized, the balancing current from one card will influence the voltage measurement on the next card due to the internal resistance in the battery cell.

The ID¹⁴ of the card is set with the seven first DIP¹⁵ switches mounted on the board. Changing the ID of the card will also make the voltage measurement software use another equation for converting the ADC register value to an actual voltage, since this have been calibrated exclusively for each card.

The eighth DIP switch enables the card to send out data reports. Due to limitations in Aros' programming software, this has to be shut off if the card needs to be reprogrammed. The data is sent every fifth second and the cards report their data 500 ms apart.

The complete list of CAN messages are specified in Table 6 and the error codes are shown in Table 7. All data reports are sent as signed, 16-bit integers which mean that they take up two bytes of data each. In case of over voltage, over current or similar, the red LED will flash to indicate that an error has occurred.

¹² Clock cycles

¹³ Proportional–integral

¹⁴ Identity

¹⁵ Dual inline package

Table 6. The complete list of CAN messages used in this project. The letter n stands for the ID of the card.

CAN message	Message ID	Data length [bytes]	Data	Unit
Data report	$0x1n$	8	1. V1 (MSB ¹⁶)	0.001 V
			2. V1 (LSB ¹⁷)	
			3. V2 (MSB)	0.001 V
			4. V2 (LSB)	
			5. Bal. current (MSB)	0.01 A
			6. Bal. current (LSB)	
			7. Temp (MSB)	0.1 °C
			8. Temp (LSB)	
Error report	$0x2n$	1	1. [Error code] see Table 7	-
Sync	$0x01$	0	-	-

Table 7. The error codes available in this project.

Error code	Meaning	Cause
0	Hardware over current error	The INT0 input was pulled low by the hardware over current protection circuit. Balancing current is bigger than ± 5 A
1	Software over current error	The balancing current is bigger than ± 4.4 A
2	Over voltage error	The voltage of V1 is bigger than 4.255 V
3	Under voltage error	The voltage of V1 is less than 2.8 V
4	Over temperature error	The temperature is bigger than 100 °C

¹⁶ Least significant bytes

¹⁷ Most significant bytes

Efficiency

Since this battery management system **transfers** energy between batteries to keep them balanced, the efficiency will be much better than systems that discharge the cells with highest voltage over a power resistor.

Measurements shows big improvements with the second card compared to the first. The tests were made by measuring the current flow to each battery cell while adjusting the balancing current. The efficiency graphs shown in Chart 13 were calculated by taking the quota between the outgoing power from one cell and the incoming power to the other cell. Since the power for all electronic components on the board is included, the efficiency will go down towards zero when no balancing current flows.

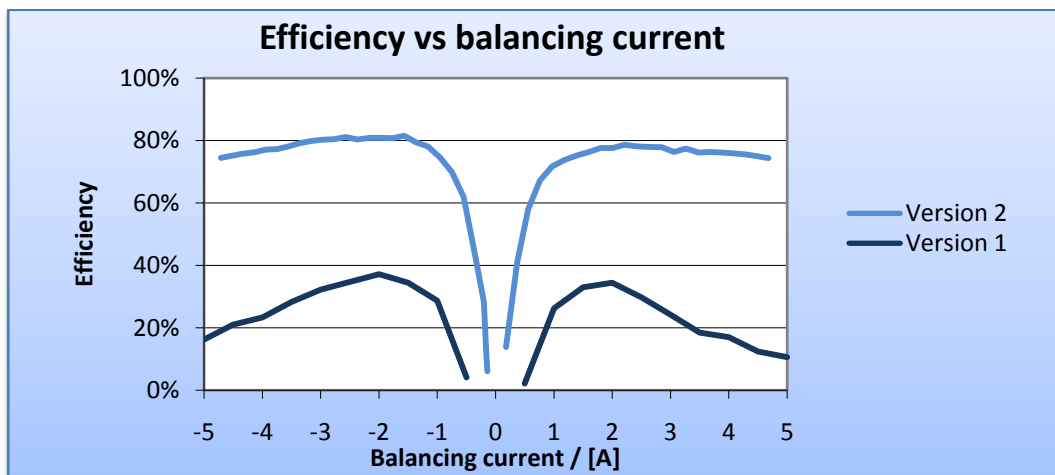


Chart 13. The efficiency when transferring power from one cell to the other. This chart is valid when the cell voltages are both 3.30 V. The better efficiency with version 2 is mostly due to less resistance on that card.

The maximum efficiency can be found at about 2-3 A. Since the resistance losses increase with the square of the current and iron losses also increase more than linearly, it is natural that the efficiency goes down when the balancing current increases.

Losses breakdown

There are several sources of losses. Some of the losses are measurable. These are, for example, the power to the on board electronics, the resistance in the path of the balancing current and the switch losses in the transistors.

The switch losses have shown to be about two per cent of the total losses and are therefore omitted in the following Chart 14. The iron losses in the inductance cannot be measured, but it is assumed to be the remaining when the previous mentioned have been subtracted from the total losses.

Refer to Chart 14 for a comparison between the two versions of the card. There is a major decrease in losses with the second version which results in the higher efficiency as shown above in Chart 13.

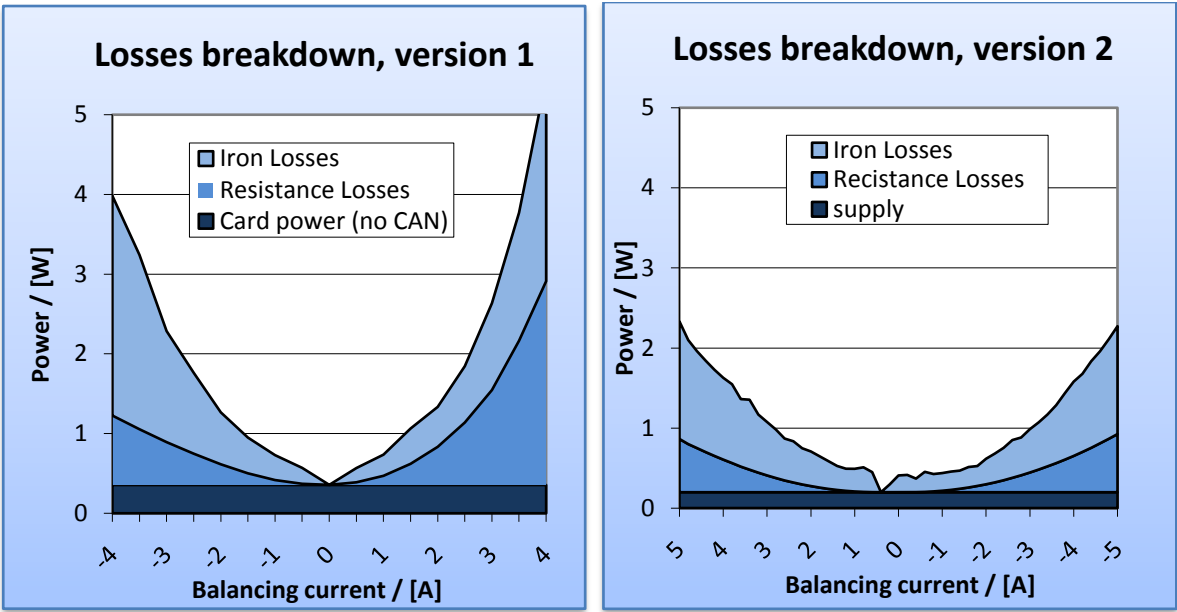


Chart 14. The charts show the distribution of the total losses. To the left, the first version of the card. To the right, the second version.

Resistances

The resistance can be broken down further. Investigating the distribution of the resistances of the first card made it possible to identify where exactly the losses arose and thus improve the efficiency for the second version. The differences in resistance for some components in the path of the balancing current and how they differ between the two versions are shown in Chart 15.

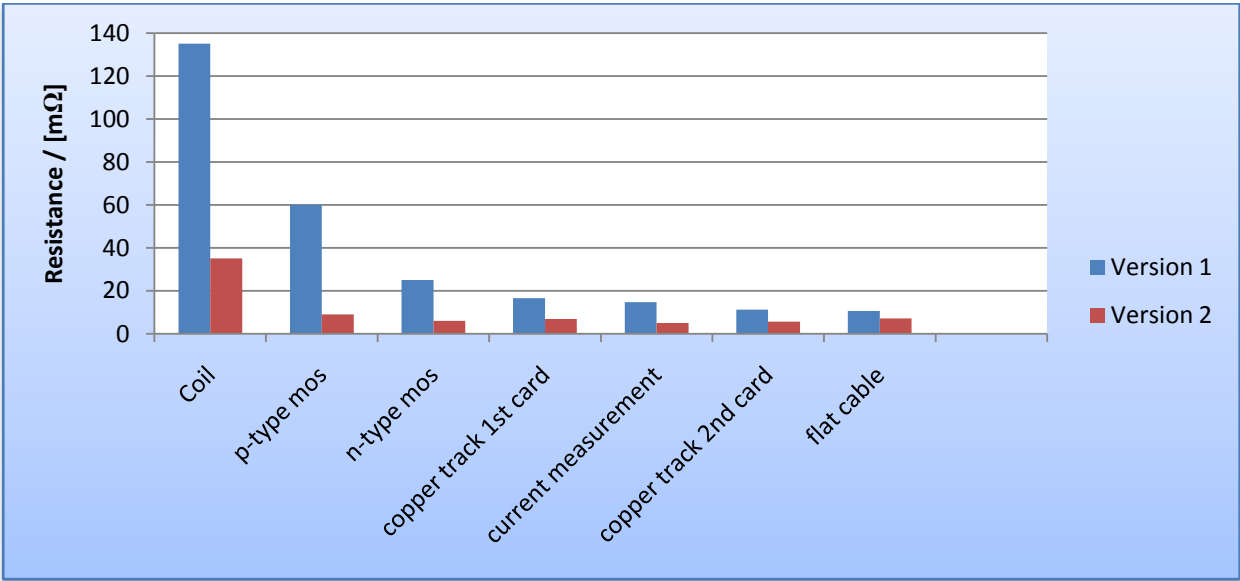


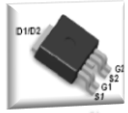

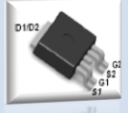
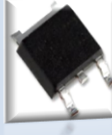




Chart 15. A comparison in resistance distribution in the path of the balancing current flow.

The major modifications that have been made to improve the second version are stated in Table 8. The overall improvement in resistance was as much as 73 %. Lower resistances are of course a good thing, but it also implies that it is more difficult to control the balancing current. This is especially true if the duty cycle resolution is low.

Table 8. A change log of what components that has been improved in the making of the second card. Only components of significance for the balancing current are shown in the table.

Component	Version 1	Version 2
Coil / inductance Improve-ment: 78 %	From Aros' stock: MSS1278-104ml (100 μ H, 1.7 A) times 4 in series/parallel. Resulting resistance: 180 m Ω 	PM2120-121K-RC (120 μ H, 5.8 A). Toroidal core. Resistance: 39 m Ω 
P-type transistor Improve-ment: 85 %	FDD8424H dual NP-MOSFET DPAK-5 R _{ds(on)} : 60 m Ω 	FDS4935BZ dual P MOSFET. (2 channels connected in parallel) SOIC8 R _{ds(on)} : 9 m Ω 
N-type transistor Improve-ment: 76 %	FDD8424H dual NP-MOSFET DPAK-5 R _{ds(on)} : 25 m Ω 	From Aros' stock: FDD8586 N MOSFET DPAK R _{ds(on)} : 6 m Ω 
Copper tracks Improve-ment: 57 %	Copper weight: 1 oz/ft ² (35 μ m) Narrow and long copper tracks on the board resulted in a total resistance of about 28 m Ω .	Copper weight: 2 oz/ft ² (70 μ m) Broad and short copper tracks due to smarter board layout resulted in a total resistance of about 12 m Ω .
Flat cable Improve-ment: 33 %	Length: 15 cm Resistance: 11 m Ω . 	Length: 10 cm Due to smarter connector positioning Resistance: 7 m Ω . 

Discussion

Determining the state of charge

The voltage of the lithium ion batteries is by no means proportional to the state of charge, SoC, of the battery. Graphs showing the voltage as a function of the SoC are provided from the manufacturer, see Appendix 1. However, these graphs may vary depending on the current flowing out or in from the cell as well as the temperature. Since the graph shown in Appendix 1 is very flat, a small variation up or down may result in a substantial change in the estimated SoC if the voltage is the only measured variable.

With these considerations in mind it is easily understood that the voltage does not give a good estimation of the battery's SoC except in the area where the batteries are almost fully charged or fully discharged. In these areas the graphs are steeper and that is why it has been possible to use the voltage as an estimation of the Soc in this project. After all, it is in the end positions that it is important to keep the cells balanced. An option could be to disable the balancing in the middle region to avoid erroneous balancing.

The way to improve the estimation of the SoC is to implement a technique called coulomb counting which means that the current to and from the battery is measured and then integrated. If it is known that the battery has a total capacity of, for example, 40 Ah, it is easy to calculate the value of the integration and consequently also the SoC.

Coulomb counting requires that the current that flows in and out of the battery is measured. The cards constructed do not have this option, but the current is measured by the motor controller circuit board and the charging power supply. This means that if the current was reported over the CAN, it would be possible to implement coulomb counting and thus getting a better estimation of the SoC in the middle region of the graph in Appendix 1. The charge and discharge characteristics for the LFP40AHA lithium ion battery which is used in this project.

Measuring the cell voltages

The accuracy of the voltage measuring circuits was required to be very high for this system to work properly. The OP Amp was required to have four amplifiers in the same package (SOIC14) so that it would not take too much space on the board. It also had to have rail to rail output capability, low offset and drift for the voltage measurement, and high bandwidth and slew rate for measuring the current ripple. It also had to be cheap since the aim for this project was to make something that was marketable in the sense of price. This combination made it very difficult to find a suitable OP Amp, but the task finally fell on the TS954.

The accuracy of the voltage measuring depended on the OP Amp and the resistors used in the differential amplifier configuration. With the components chosen the maximum

difference between the estimated linear equation and the actual voltage was 20 mV, even when separate linear equations were used for each card.

The accuracy could have been improved by using a better OP Amp and to use resistors with 0.1% tolerance instead of 1%. This would give better similarity between circuits as well as better line fitting. The reason that low tolerance resistors were not used in this project was the price; thin film (0.1 %) resistors are about ten times more expensive compared to thick film (1 %).

Current measurements

Since the accuracy of the current measurements does not have to be as precise as the voltage measuring, the use of 1% resistors is sufficient. The current measuring works nicely and gives the same result as when the current is measured using a current clamp meter.

The synchronous sampling of the current gives almost exactly the same result as the second ADC channel which measures the average current through a low pass filter according to Appendix 2. The difference is no more than 20 mA which is very satisfactory.

Since the gain of the differential amplifier measuring the current was redesigned to 97.6 in the second version of the card, the software is very quick in converting the ADC register value to the actual current. Take wisdom in this; always design the hardware so that it simplifies the software.

Transistor losses

There is much less on-resistance in an N-type transistor compared to a P-type. Therefore, it was desirable to use N-type transistors at both the high-side and the low-side. To drive the high side N-transistor, a boost up, gate driver would have to be used.

All these drivers have an under voltage shutdown functionality which is activated at about 8-9 V. The problem is that the maximum available voltage at one module ranges from 5 V to 8.5 V. This meant that it would have been necessary to build a step-up voltage converter to be able to use the boost-up drivers.

Since the space is very limited on the board and due to the lack of time, the decision was taken to use a P-type MOSFET at the high-side and to use an ordinary MOSFET gate driver IC.

Budget

The costs for this project are shown in Table 9. The components have been cheap since most of the components were available from Aros' stock. The prices of each component will not be declared in this report due to secrecy, but the total component cost can be stated.

The most costly components have been the inductor and the digital isolator used for CAN. The R8C23 were sponsored by Renesas who seemed to find this project very interesting.

Table 9. The costs associated with this project.

	Cost in US dollars
10 lithium ion batteries, 40 Ah	\$ 710
Electronics components for 9 cards	\$ 110
10 boards from PCBCart.com	\$ 110
Sum	\$ 930

CAD¹⁸

Software at Aros made it possible to generate a 3D image of the circuit board layout. Of course, this had to be tested and while in the field, I also drew a 3D model of the battery. The result can be seen below in Figure 20.

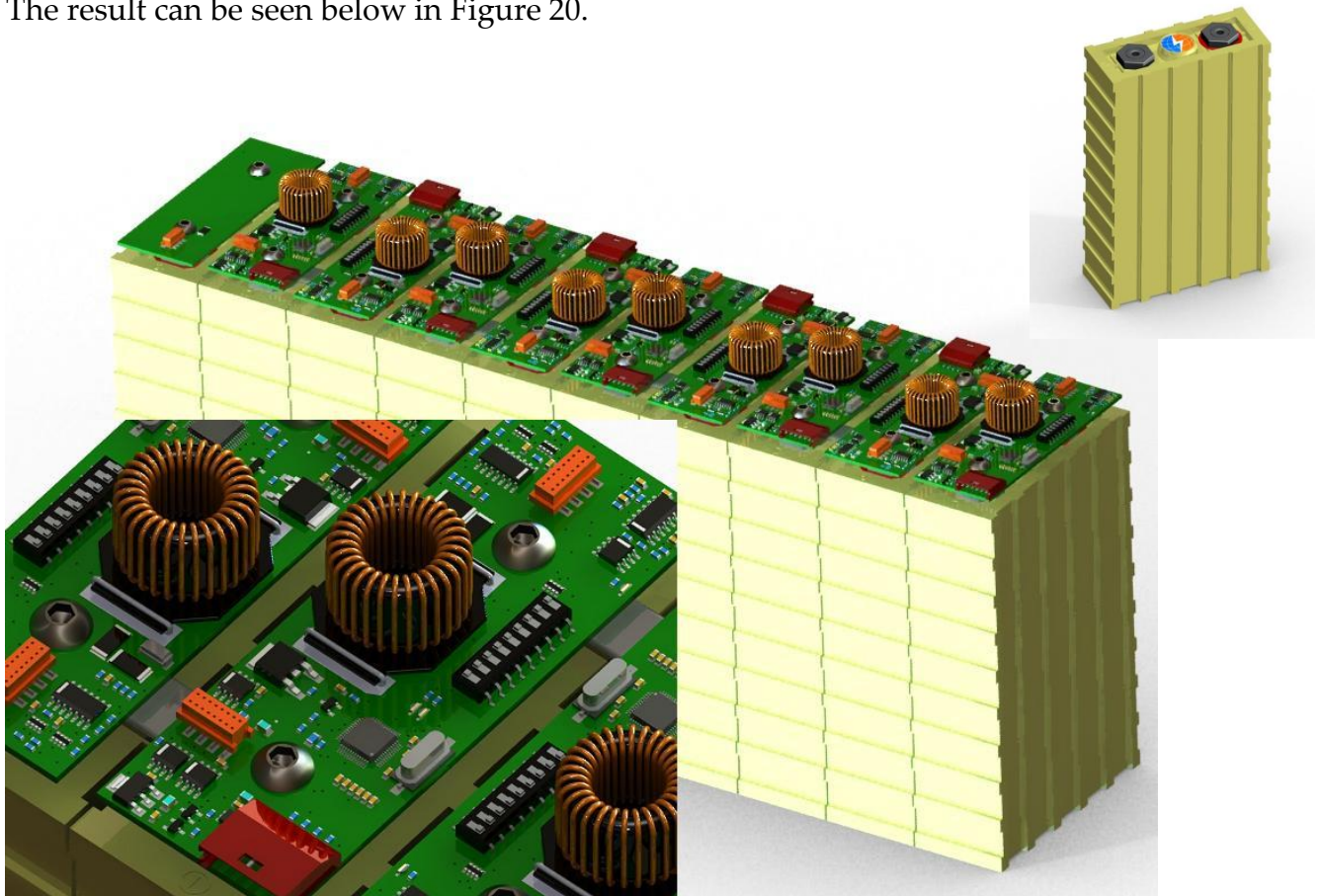


Figure 20. A 3D image of the cards generated with Solid Works.

¹⁸ Computer aided design

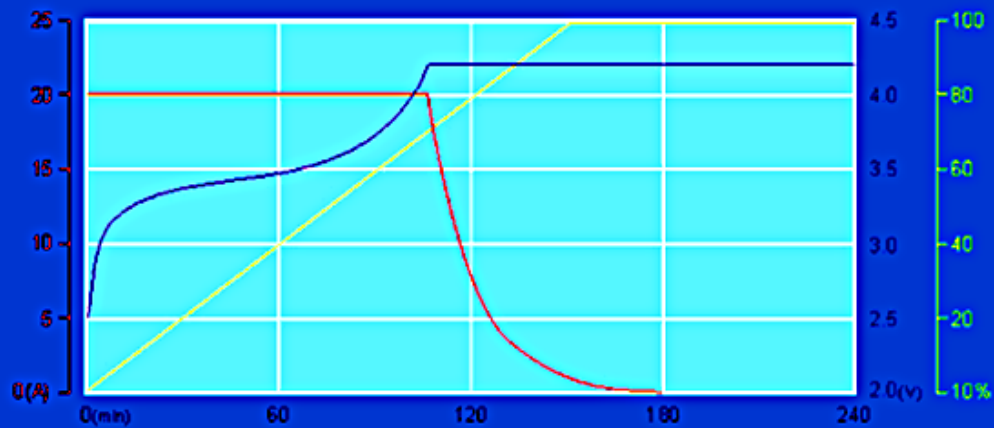
References

1. Aros Electronics. [Online] 2008. <http://www.aros.se/company-nf.html>.
2. *Instruction Manual for LFT/LCP/LMP Lithium Power Battery*. China : Thunder Sky Battery Limited, 2008.
3. **Staff at Aros Electronics AB**. 2008.
4. <http://www.madkatz.com/ev/batteryTechnologyComparison.html>, **Clasohlson and Wikipedia**.
5. *Dynamic charge equalisation for series-connected batteries*. **Moo, C.S.** 5, Taiwan : IEE Proc.-Electr. Power Appl., 2003, Vol. 150.
6. *Two-Stage Cell Balancing Scheme for Hybrid Electric Vehicle Lithium-Ion Battery Strings*. **Park, Hong-Sun, o.a.** 2007, IEEE, Power Electronics Specialists Conference, ss. 273 - 279.
7. *Design considerations for charge equalization of an electric vehicle battery system*. **Kutkut, N.H., o.a.** Jan-Feb, Middleton, USA : IEEE, 1999, Vol. Transactions on Industry Applications.
8. *A PWM controlled simple and high performance battery balancing system*. **Nishijima, K., Sakamoto, H. och Harada, K.** Kumamoto, Japan : IEEE Power Electronics Specialists Conference, 2000, Vol. 1.
9. **Jan Williams, Mark Thoren**. *Developments in Battery Stack Voltage Measurement*, . u.o. : Linear technology, 2007. Application Note 112.
10. Digital isolations: Interface. [Online] Analog Devices. <http://www.analog.com/en/interface/digital-isolators/products/index.html>.

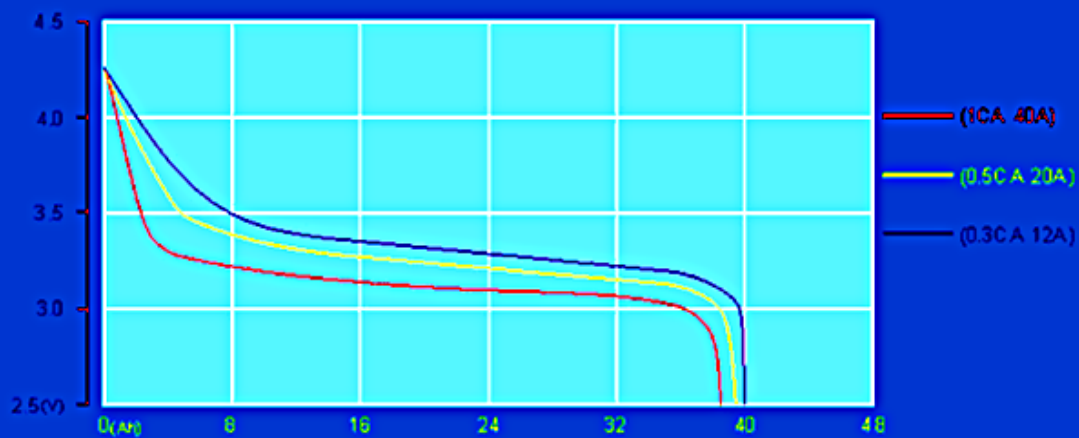
Appendix

Appendix 1. The charge and discharge characteristics for the LFP40AHA lithium ion battery which is used in this project.

TS-LFP40AHA型電池の充放電特性
TS-LFP40AHA CHARGE & DISCHARGE CHART

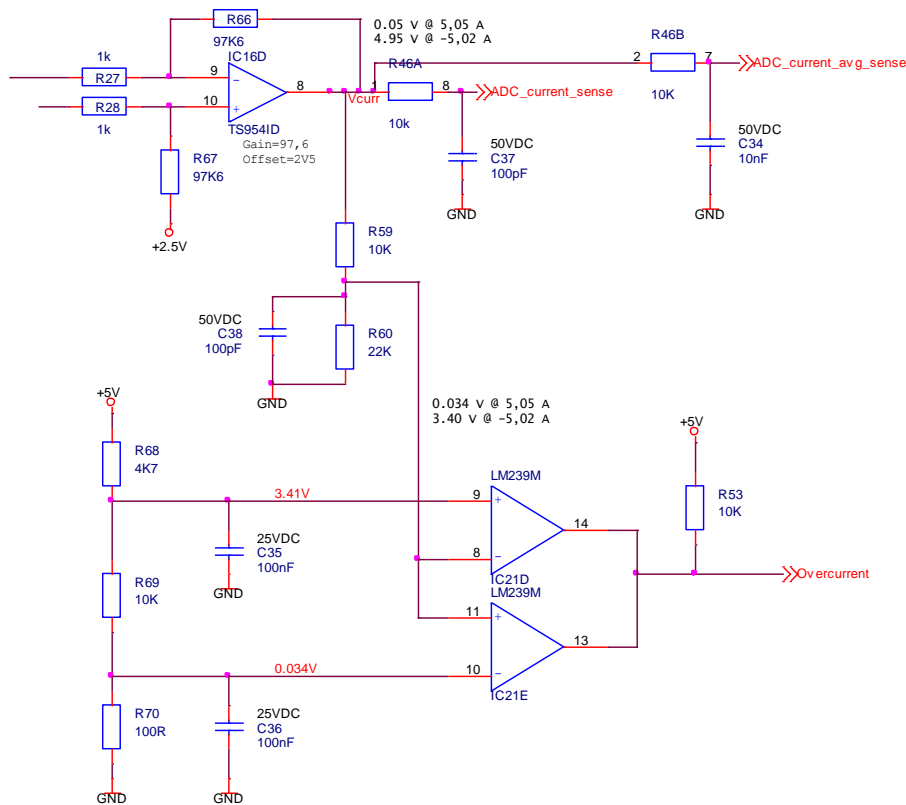


TS-LFP40AHA在25℃環境下的充電特性
TS-LFP40AHA CHARGE AT TEMPERATURE OF 25℃

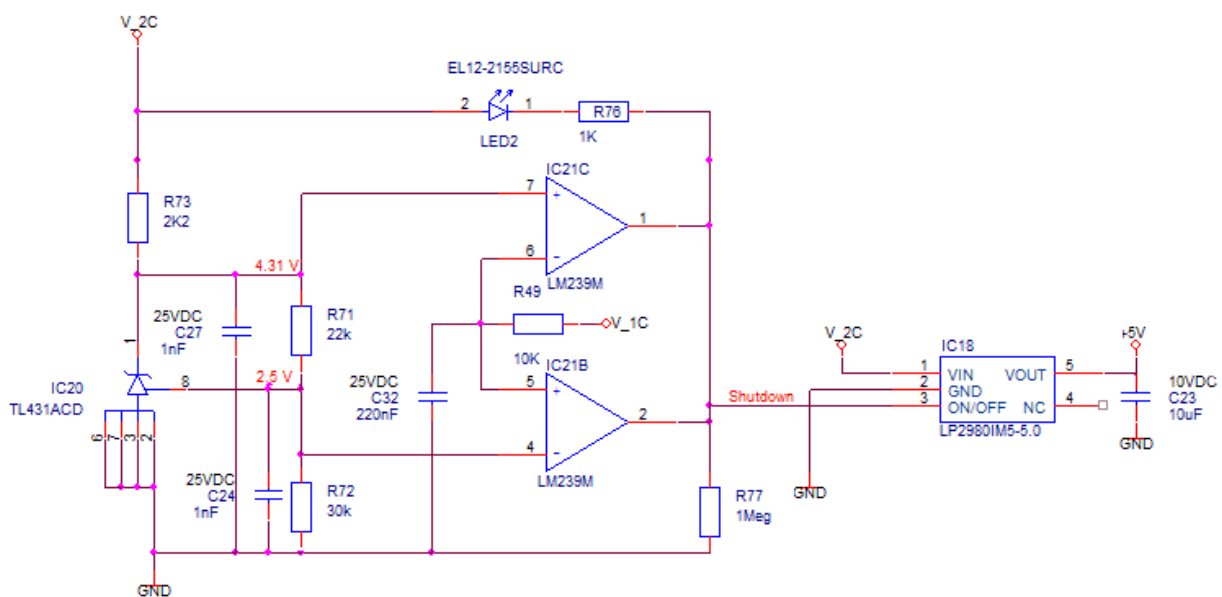


TS-LFP40AHA在25℃環境下的放電特性
TS-LFP40AHA DISCHARGE AT TEMPERATURE OF 25℃

Appendix 2. The current measuring and over current protection circuits. The voltage over the shunt resistor is input at the top left (to R27 and R28). The two different low pass filters, R46A/C37 and R46B/C34 gives a cutoff frequency of 1600 kHz and 1.6 kHz, respectively.

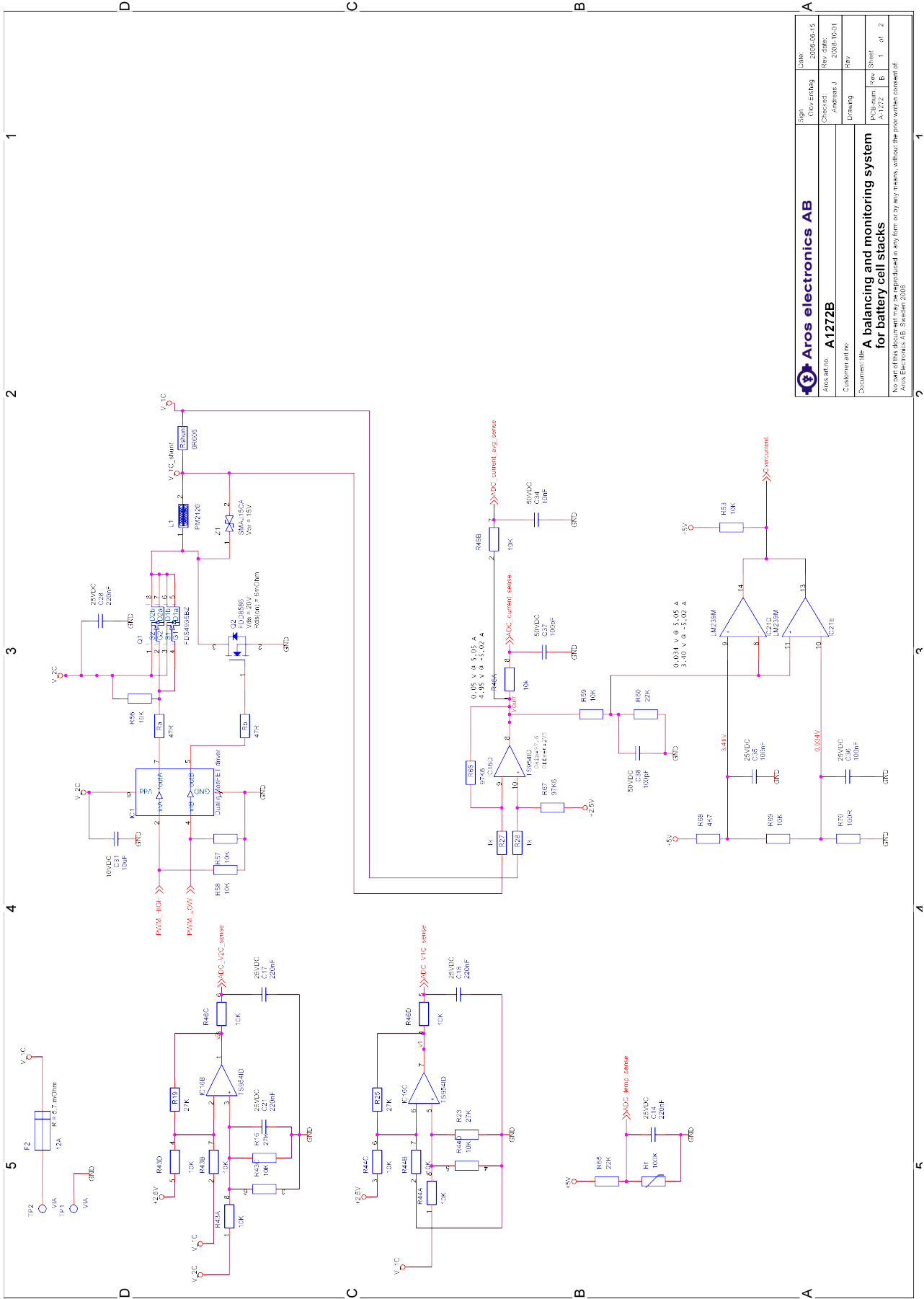


Appendix 3. The over/under voltage protection circuits. The *shutdown* signal is pulled down through the LED which then will light in case of one of the OCO¹⁹ comparators activates. IC20 creates the reference voltages, 4.31 V and 2.5 V, that are compared with V_{1C}. If V_{1C} is out of range, the voltage regulator is shut off. The voltage regulator feeding the CAN modules is only mounted on the first card and is therefore omitted in this figure.



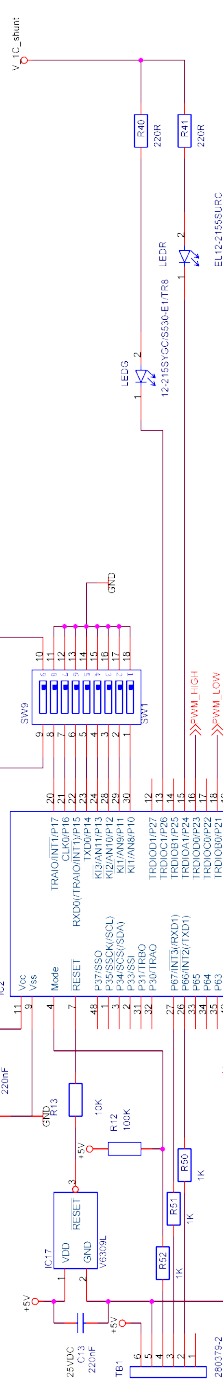
¹⁹ Open collector output

Appendix 4. The whole circuit diagram for this project. Two pages.



Aros electronics AB		Sign	Obv. ending	Date:
A1272B		Checked:	Rev. date:	2008-09-15
Customer art no.		Drawing	Rev.	2008-10-01
Document title		PCB-art no.	Rev.	Rev.
A balancing and monitoring system for battery cell stacks		A-1272	B	1 of 2
No part of this document may be reproduced in any form or by any means, without the prior written consent of Aros Electronics AB, Sweden 2008				

5 4 3 2 1



EL12155SURC

SW1

SW2

SW3

SW4

SW5

SW6

SW7

SW8

SW9

SW10

SW11

SW12

SW13

SW14

SW15

SW16

SW17

SW18

SW19

SW20

SW21

SW22

SW23

SW24

SW25

SW26

SW27

SW28

SW29

SW30

SW31

SW32

SW33

SW34

SW35

SW36

SW37

SW38

SW39

SW40

SW41

SW42

SW43

SW44

SW45

SW46

SW47

SW48

SW49

SW50

SW51

SW52

SW53

SW54

SW55

SW56

SW57

SW58

SW59

SW60

SW61

SW62

SW63

SW64

SW65

SW66

SW67

SW68

SW69

SW70

SW71

SW72

SW73

SW74

SW75

SW76

SW77

SW78

SW79

SW80

SW81

SW82

SW83

SW84

SW85

SW86

SW87

SW88

SW89

SW90

SW91

SW92

SW93

SW94

SW95

SW96

SW97

SW98

SW99

SW100

SW101

SW102

SW103

SW104

SW105

SW106

SW107

SW108

SW109

SW110

SW111

SW112

SW113

SW114

SW115

SW116

SW117

SW118

SW119

SW120

SW121

SW122

SW123

SW124

SW125

SW126

SW127

SW128

SW129

SW130

SW131

SW132

SW133

SW134

SW135

SW136

SW137

SW138

SW139

SW140

SW141

SW142

SW143

SW144

SW145

SW146

SW147

SW148

SW149

SW150

SW151

SW152

SW153

SW154

SW155

SW156

SW157

SW158

SW159

SW160

SW161

SW162

SW163

SW164

SW165

SW166

SW167

SW168

SW169

SW170

SW171

SW172

SW173

SW174

SW175

SW176

SW177

SW178

SW179

SW180

SW181

SW182

SW183

SW184

SW185

SW186

SW187

SW188

SW189

SW190

SW191

SW192

SW193

SW194

SW195

SW196

SW197

SW198

SW199

SW200

SW201

SW202

SW203

SW204

SW205

SW206

SW207

SW208

SW209

SW210

SW211

SW212

SW213

SW214

SW215

SW216

SW217

SW218

SW219

SW220

SW221

SW222

SW223

SW224

SW225

SW226

SW227

SW228

SW229

SW230

SW231

SW232

SW233

SW234

SW235

SW236

SW237

SW238

SW239

SW240

SW241

SW242

SW243

SW244

SW245

SW246

SW247

SW248

SW249

SW250

SW251

SW252

SW253

SW254

SW255

SW256

SW257

SW258

SW259

SW260

SW261

SW262

SW263

SW264

SW265

SW266

SW267

SW268

SW269

SW270

SW271

SW272

SW273

SW274

SW275

SW276

SW277

SW278

SW279

SW280

SW281

SW282

SW283

SW284

SW285

SW286

SW287

SW288

SW289

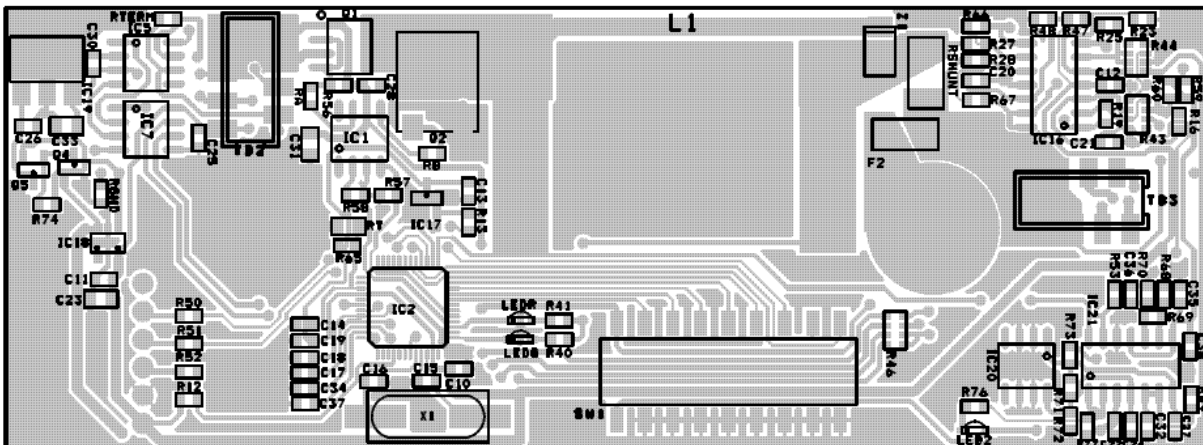
SW290

SW291

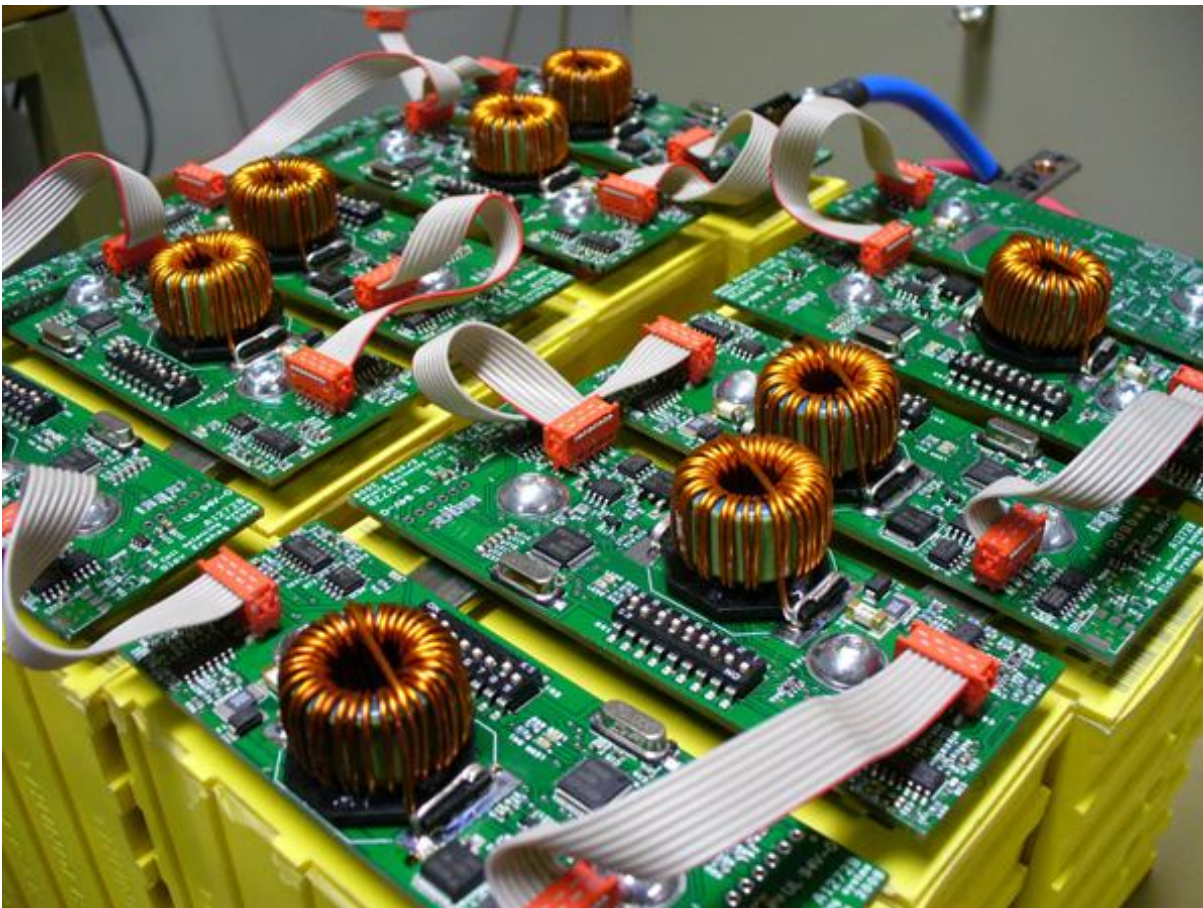
Appendix 5. The list of components used in the second version.

Number	Count	Name	Value
1	16	C10,C11,C12,C13,C14,C17, C18,C19,C20,C21,C22,C25, C26,C28,C30,C32	220nF
2	2	C15,C16	22pF
3	3	C23,C31,C33	10uF
4	2	C24,C27	1nF
5	1	C34	10nF
6	2	C35,C36	100nF
7	2	C37,C38	100pF
8	1	F2	12A
9	1	IC1	Dual n MOSFET driver
10	1	IC2	R8C23
11	1	IC5	AMIS42665AGA
12	1	IC7	ADuM1201BRZ
13	1	IC16	TS954ID
14	1	IC17	V6309L
15	1	IC18	LP2980IM5-5.0
16	1	IC19	LM2937-5.0
17	1	IC20	TL431ACD
18	1	IC21	LM239M
19	1	LEDG	12-215SYGC/S530-E1/TR8
20	2	LED2,LEDR	EL12-2155SURC
21	1	L1	PM2120
22	1	Q1	FDS4935BZ
23	1	Q2	FDD8586
24	1	Q4	BSS123
25	1	Q5	Si2309DS-T1
26	2	Rb,Ra	47R
27	1	Rgnd	0R
28	1	Rshunt	0R005
29	1	Rterm	120R
30	2	R12,Rt	100K
31	13	R13,R43,R44,R46,R47,R48, R49,R53,R56,R57,R58,R59, R69	10K
32	5	R16,R19,R23,R25,R71	27K
33	6	R27,R28,R50,R51,R52,R76	1K
34	2	R40,R41	220R
35	2	R60,R65	22K
36	2	R66,R67	97K6
37	1	R68	4K7
38	1	R70	100R
39	2	R72,R74	39K
40	1	R73	2K2
41	1	R77	1Meg
42	1	SW1	SW9
43	1	TB1	280379-2
44	2	TB2,TB3	7-188275-8
45	2	TP1,TP2	VIA
46	1	X1	20MHz
47	1	Z1	SMAJ15CA

Appendix 6. The layout of the second version of the card. Only the component placement and the top layers are shown.



Appendix 7. A picture of the battery pack with all nine balancing card mounted.



Appendix 8. A picture of my mentors at Aros Electronics. From the left. Mikael Alatalo, electric motor expert and head mentor, Andreas Johansson, hardware design expert and Josef Gårdstam, software programming expert.

